TE Technology Department

Magnets, Superconductors and Cryostats
TE-MSC

June 2012
Internal Note 2012-11
EDMS Nr: 1214775

Design of the Anti-Solenoid System for the CLIC SiD Experiment

Authors: A. Bartalesi, M. Modena

Keywords: Anti-Solenoid, CLIC, SiD, ILD, Experiment, QD0

Abstract

In the CLIC SiD experiment design baseline, with the machine parameter L^* set to 3.5 m, the final focus quadrupole QD0 will be placed *inside* the detector itself. This configuration is very challenging by an integration point of view.
Among several other aspects, the iron-dominated QD0 and the incoming beams will need an active magnetic shielding to avoid unacceptable interactions with the magnetic field generated by the main solenoid of the detector.
According to the baseline design, this shielding is provided by a superconducting anti-solenoid, and this note aims to describe the procedure followed to design it.

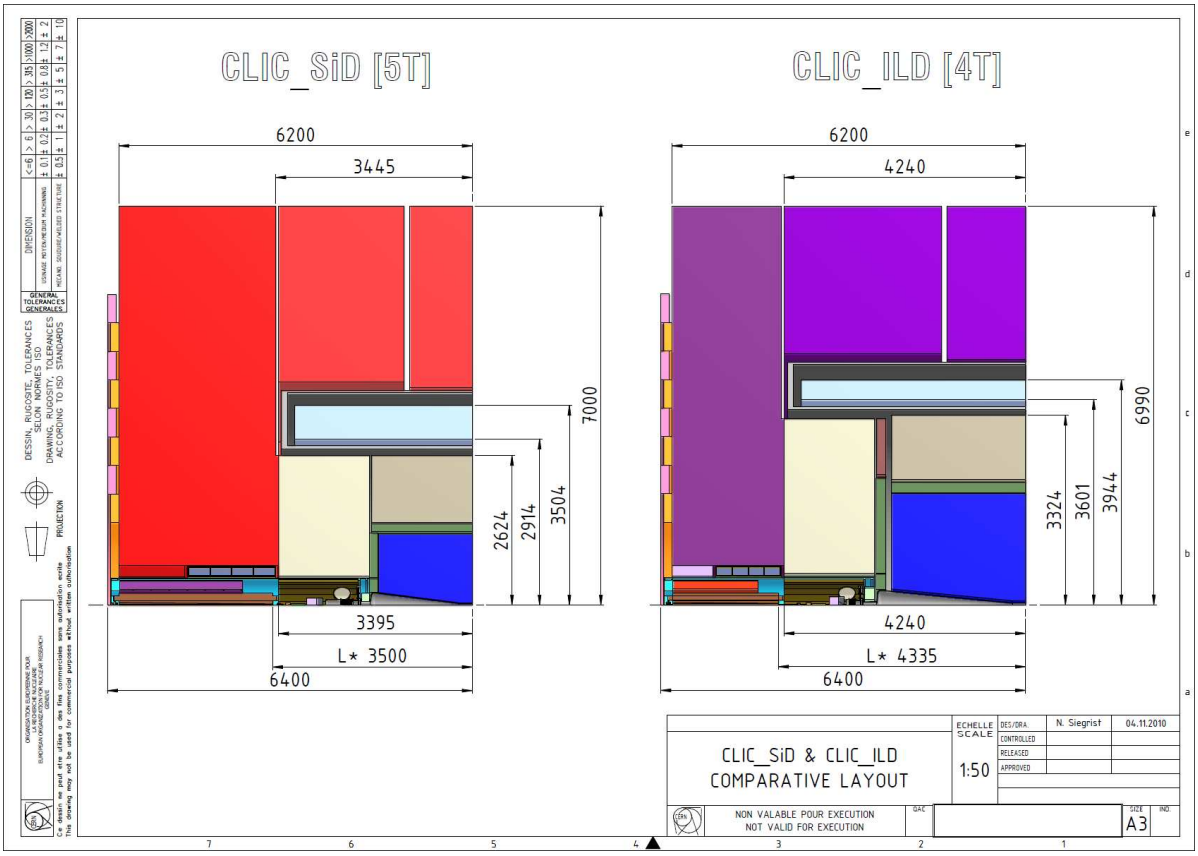

Figure 1: The CLIC SiD and CLIC ILD designs overview.

1. Introduction

Two experiments and two detectors are proposed in the current CLIC baseline scenario [1]: the Silicon Detector CLIC SiD and the International Large Detector CLIC ILD, both shown in figure 1. The CLIC SiD is considered to be the most challenging one, because of its higher magnetic field of 5 T at the Interaction Point, or IP; therefore the following study focuses on the CLIC SiD design only, assuming that it would be easier to adapt the conclusions of this study to the CLIC ILD case.

With an L^* value of 3.5 m [1, p. 44], the normal conducting final focus quadrupole (also referred as QD0) lies *within* the boundaries of the detector as shown in figure 2. This magnet is based on a hybrid design [2]: it is constituted by a traditional set of air-cooled copper coils inducing a field into the ferromagnetic yoke and poles, with the addition of several permanent magnet blocks, needed to increase the achievable maximum gradient. In such a compact detector configuration this magnet could be negatively affected by the main solenoid magnetic field, in two different ways: the detector field could saturate the ferromagnetic parts of the final focus, and also demagnetize its permanent magnet blocks, in both cases leading to a degradation of the level and quality of the quadrupolar field gradient.

Finally, relevant magnetic forces would act on QD0 in case it gets magnetized by the

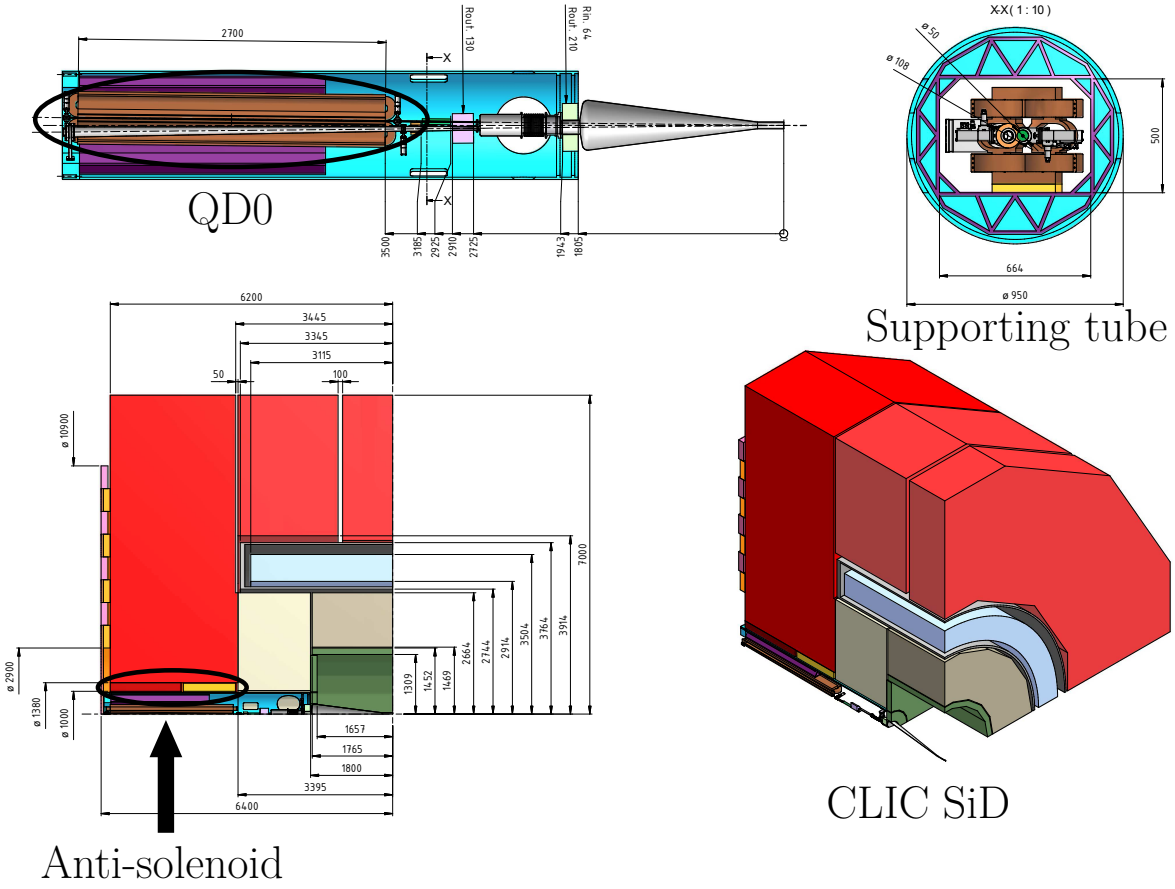

Figure 2: The CLIC SiD layout.

main solenoid, making its stabilization and alignment more difficult.
To prevent all of that, it was proposed since 2009 an active magnetic shielding (i.e. *anti-solenoid* [3]) to expel the solenoidal magnetic field from the region reserved to the final focus quadrupole, and therefore avoid any magnetic cross-talk between the main solenoid of the detector and QD0.
The anti-solenoid must then be dimensioned and integrated in the complex layout of the CLIC SiD Machine Detector Interface or MDI. The aim of this note is to describe how the anti-solenoid system was designed, explaining the process followed to determine its coils number, their shape, placement and operating currents. Before presenting the final design proposed for the anti-solenoid, a number of intermediate designs are illustrated, to better explain how this study evolved, reporting the issues solved at every step, the feedbacks received from the colleagues and the results obtained with the FEM simulations.

1.1. The CLIC SiD experiment and the MDI

The MDI region of the CLIC SiD detector includes various components belonging to different machine and detector subsystem, therefore the integration process is one of

the most challenging task in the anti-solenoid design process. Figure 2 shows the components which are the most relevant to this study. Among them there are the QD0 quadrupole, its supporting, alignment and stabilization systems, the hadronic calorimeter, the electromagnetic calorimeter, the beam feedback instrumentation, the vacuum pipes, the post collision line etc...
In the magnetic simulations, the following items were *always* taken into account and modelled:

- The main solenoid.
- The flux-return yoke.
- The anti-solenoid.

While the following ones were considered only in some design steps and relative simulations:

- The supporting tube, to investigate the option of a ferromagnetic material.
- An ferromagnetic disc, to be placed in front of QD0 to better shield its innermost part.
- The QD0 quadrupole, since it can be included only in the most advanced 3D simulations.

Any other element was considered as non magnetic, then they were not included in the simulations, even though they were considered in the overall MDI integration study.

1.2. Starting of the anti-solenoid design

The study presented by D.Swoboda [3], which is probably the first document mentioning a CLIC anti-solenoid, was also the starting point of our study. Figure 3a shows the proposed layout for the CLIC ILD detector, while figure 3b illustrates the flux lines obtained when simulating the CLIC SiD detector equipped with the first version of the anti-solenoid.
The configuration showed above was used for the earlier beam dynamic simulations, but for this study we defined a brand new anti-solenoid layout, based on a different set of dimensions and operating parameters. In other words, the older design presented above were used only as concepts to define the anti-solenoid which was being studied and improved during this study.

1.3. Objectives

Considering all the above, at the time this study started, the main objectives were defined as:

1. To dimension an anti-solenoid capable to provide the correct magnetic shielding of the final focus quadrupole QD0.

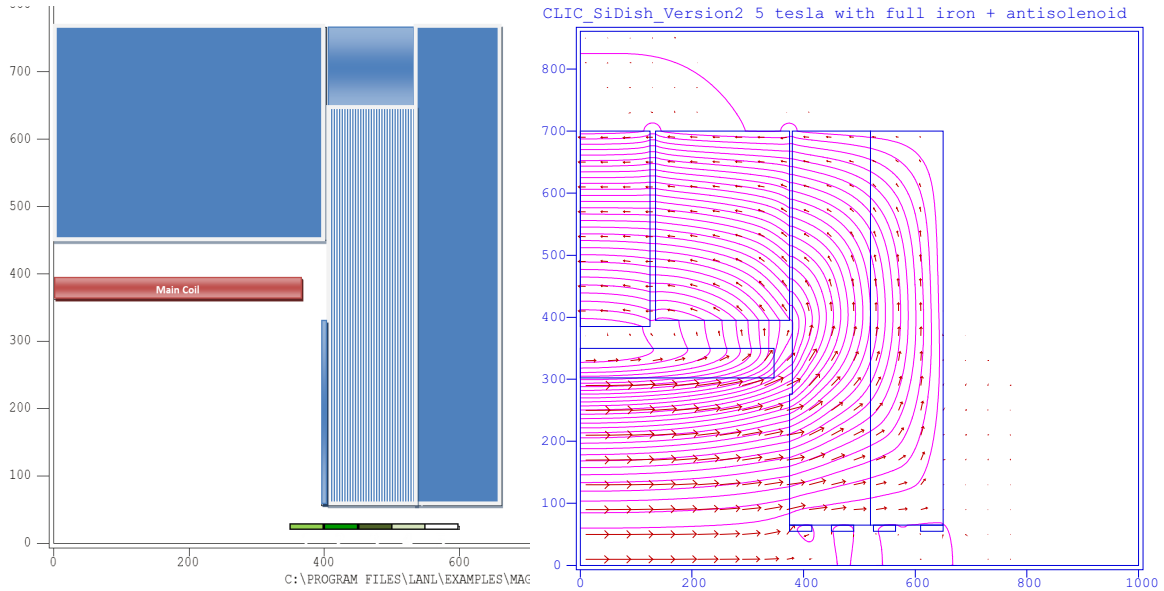

(a) Antisolenoid concept in CLIC ILD.

(b) Flux lines in the CLIC SiD detector and anti-solenoid.

Figure 3: The previous status of the anti-solenoid.

2. To ensure that the field profile in the incoming beam region, and particularly on the beam axis, is acceptable by a beam dynamic point of view.

3. To make sure that the proposed design of the anti-solenoid is compliant with every other system and component of the MDI, and eventually participate in the integration process.

The output of this study was then defined as the complete set of dimensions necessary to define the anti-solenoid. This includes firstly the number of coils to be used, and then for each one of them:

dimensions which are length, inner radius and thickness in case of the simplest shape,

position or distance from the coil center to the IP, since the anti-solenoid is coaxial with the main solenoid,

current expressed in A·turns, or current density.

2. The two-dimensional model

In the earliest stage of this study A 2D axial-symmetric FEM model was adopted. This kind of models in fact are fast to set-up and simulate, easy to modify, and they can give results in terms of magnetic field, magnetic forces and even mechanical stress acting on

the coils of the anti-solenoid. Even if QD0 cannot be introduced in such model, and the detector yoke is not perfectly axial-symmetric (its profile is dodecahedral rather than circular), it was possible to use efficiently such model to minimize the field in the area reserved to QD0, and also to evaluate the forces and even the stresses induced on the anti-solenoid coils by the magnetic fields.
In other words, it was considered more efficient to start with such a simple yet meaningful model to define a first design of the anti-solenoid, switching to the more complex and time consuming 3D simulations only after having a preliminary, yet realistic, anti-solenoid design and a more mature and advanced MDI layout.

2.1. The Ansys model

The first finite elements software to be used was Ansys™ by Ansol, mainly because such program allows to evaluate forces and stresses acting on the anti-solenoid after performing the magnetic simulation.
The whole analysis in fact occurs in two steps: in the first part the magnetic field and Lorentz forces are evaluated, while in the second part the magnetic forces previously evaluated are used as loads to compute the stresses and deformation of the anti-solenoid coils.
The element type used in the first part is the `PLANE13`, a 2-D Coupled-Field Solid [4], with the option of axial-symmetry. A second symmetry is exploited, as the field on the vertical plane passing through the IP has to be perpendicular to the plane itself. These two symmetries allow to model just a quarter of the detector axial section.
The only element load are the current densities, applied on the section of each coil constituting either the anti-solenoid or the main solenoid. The element correctly considers those current densities as perpendicular to its own plane.
The flux-return yoke is defined as a ferromagnetic region, and its B-H curve is reported in appendix A. This curve corresponds to a mild average carbon steel, with a permeability reduced by a factor 0.8 to take into account that the real flux return yoke will have some slots to host the muon trackers and other devices, so it will not be just a bulk block of steel. The relative permeability of every other material (air and superconducting cables) was set to 1.
Due to the presence of iron regions, a non linear analysis is needed to determine the resulting magnetic flux. This first analysis gave two important magnetic results: the magnetic field on the beam axis and the resulting Lorentz forces acting on the coils. Such forces are evaluated at each node and stored in memory, to be available for the second step of the analysis, while the field profiles on the beam axis were plotted and sent to the beam physics colleagues to check the compatibility with the beam dynamic.
The second part of the analysis consists in a mechanical simulation. The previous elements are deleted and a new mesh is created, matching the exact position and ordering numbers of the nodes, but only the coils are re-meshed, while all the others surrounding regions are deleted. The element type used is now the `PLANE42`, a 2-D Structural Solid, with the option of axial-symmetry. This new mesh is easily loaded with the stored nodal Lorentz forces and since the nodes numbers and positions are exactly the same as in

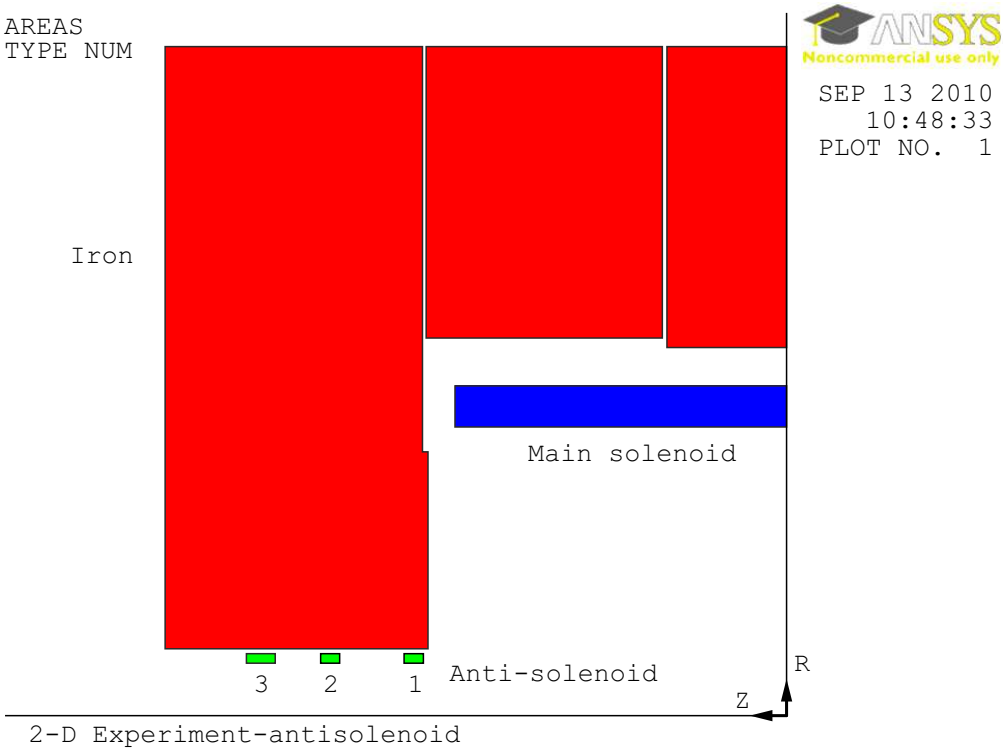

Figure 4: The first finite element model of the SiD, using Ansys™.

the previous mesh, this passage can be done directly, without any further adaptation. Finally, a boundary condition of "no displacement" is set on a flat face of each coil, to constrain its axial displacement. On the radial direction the coils are free to expand, so that the radial forces are balanced by the hoop stress only. With this kind of analysis a stress map is obtained for each coil, as well as the axial forces, given as the sum of the support reactions. The main assumption is that the coil is made of a continuous, homogeneous, linear and isotropic material and its properties are: $E = 70$ GPa and $\nu = 0.3$.

The geometry used for the detector was the one provided by the colleagues from the CLIC SiD design working group. This geometry changed during the whole evolution of the anti-solenoid dimensioning analysis, and this is explained later in detail. At this stage is important to mention that the value of L^*, which from the MDI point of view is considered as one of the most relevant, was set to 3.8 m (as a reminder this value was set to 3.5 m in the final version of the experiment design).

For the anti-solenoid geometry, it was proposed a new design, made by just 3 superconducting coils, as shown in figure 4. The coils have an inner radius of 0.55 m, and an outer radius of 0.65 m. Lengths are 0.2 m for coils 1 and 2 and 0.3 m for coil 3. The current densities have been set to $1.14{\cdot}10^8$ A/m^2, $3.67{\cdot}10^7$ A/m^2 and $6.00{\cdot}10^6$ A/m^2 respectively for coil number 1, 2 and 3.

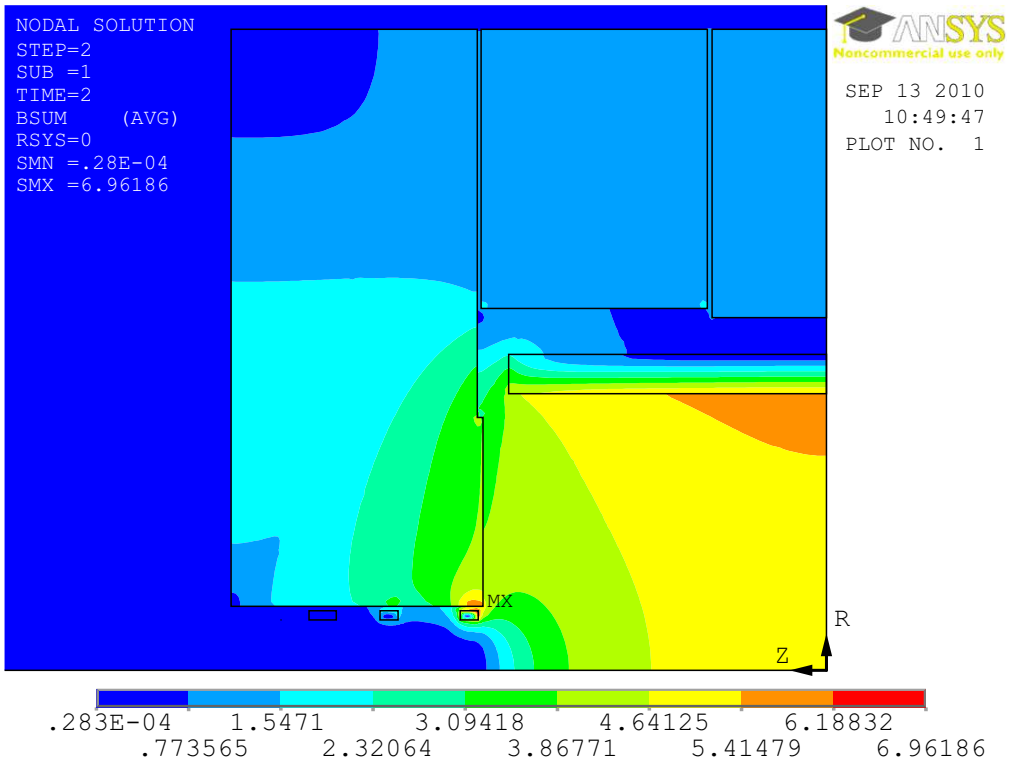

Figure 5: Resulting magnetic field modulus $|\mathbf{B}|$ on the detector model.

2.2. Results of the Ansys model

In terms of absolute value of the remaining magnetic field in the QD0 region, the newly designed anti-solenoid performs better than the previous version. Figure 5 shows the intensity of the magnetic flux in the whole detector, while figure 6a represents the magnetic field along the beam axis, from the Interaction Point up to 10 m away from it. Its components B_z and B_r, respectively the axial and radial components of the field, are expressed in the coordinate system of the detector. It is important to remind that the beam axis is inclined by an angle of 0.01 rad with respect to the detector axis. A zoom in the QD0 region is shown in figure 6b.

From the mechanical point of view, there are a few observation to be done: the most loaded coil of the whole anti-solenoid, is the first, which is the innermost, or closest to the IP. In the second coil, all the forces and stresses drop by more than a factor ten, and even more in the third coil. So considering that we were mainly interested in the feasibility of such a solution, it was considered sufficient to study in high detail only the first coil. The mechanical simulation pointed out that this coil is loaded in the negative radial direction, in other words has a tendency to collapse on itself, which can lead to instability issues like buckling. Also, the coaxial configuration of solenoid and anti-solenoid is not a stable one, and an angular error between the two axes will result in an destabilizing torque acting on both the electromagnets, pushing them in a way to

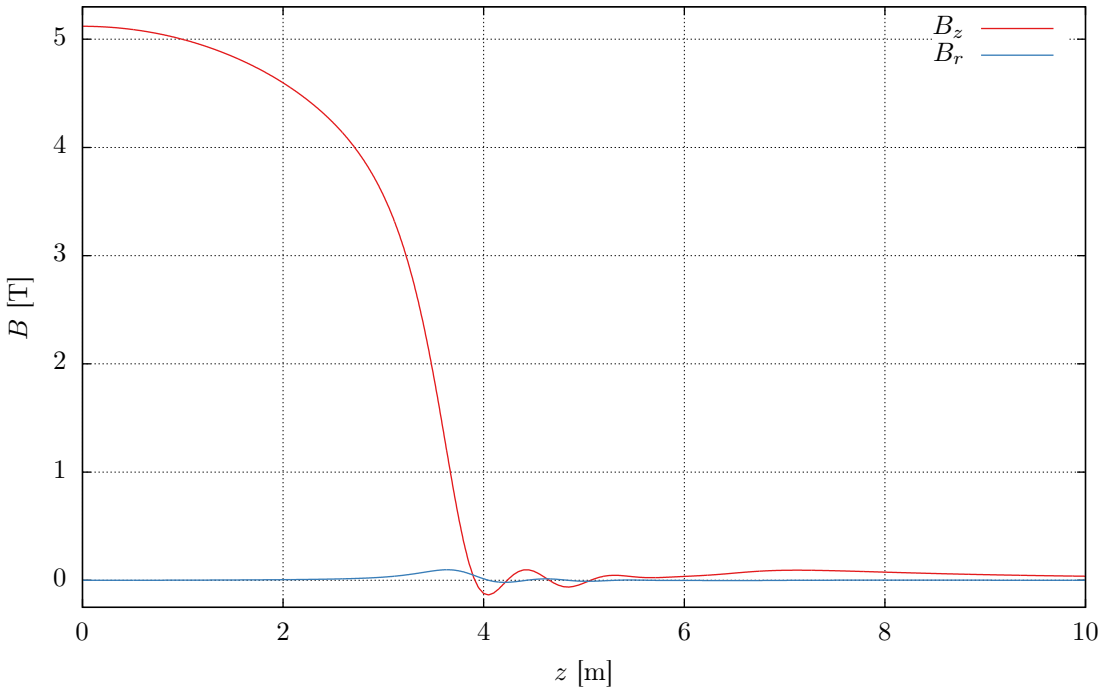

(a) Axial and radial magnetic from the IP to 10 m away.

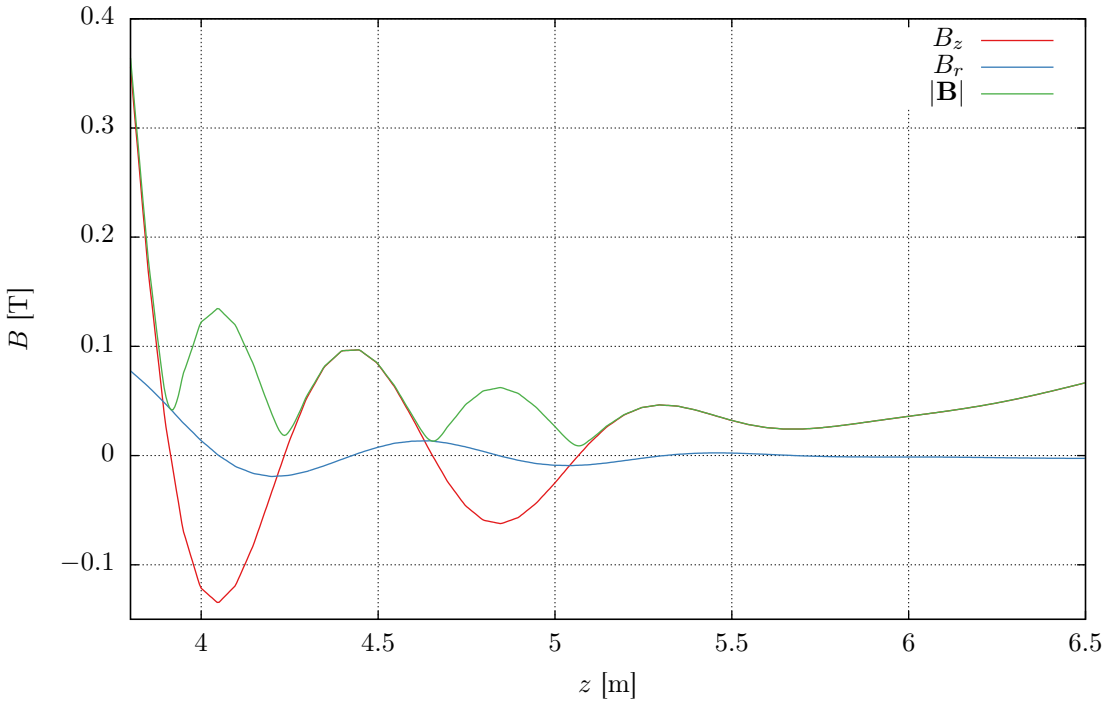

(b) A zoom of $|\mathbf{B}|$, B_z and B_r in the QD0 region.

Figure 6: Resulting magnetic field on the beam line.

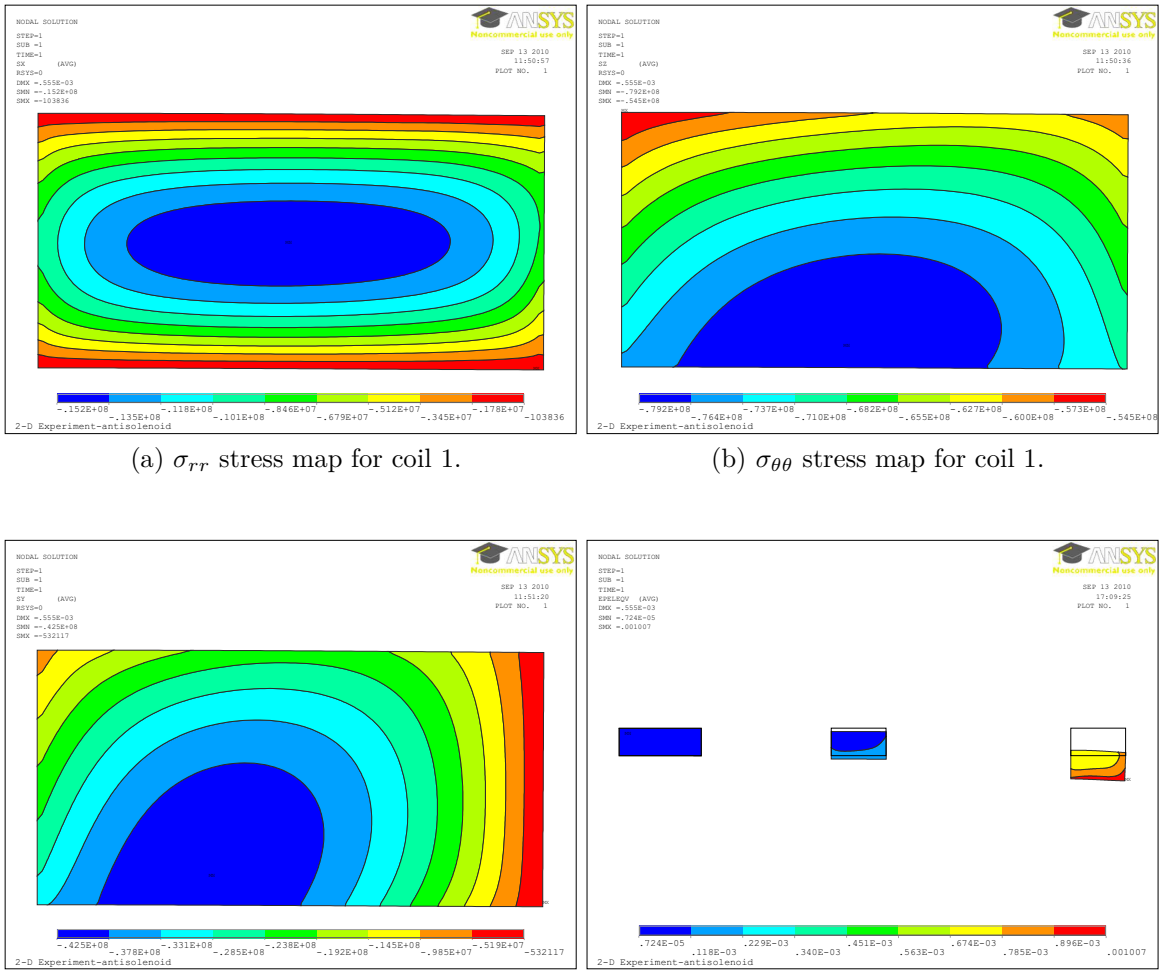

(a) σ_{rr} stress map for coil 1.

(b) $\sigma_{\theta\theta}$ stress map for coil 1.

(c) σ_{zz} stress map for coil 1.

(d) ϵ_{eq} strain map for coils 1 2 and 3.

Figure 7: Stress and deformation estimation from Ansys™.

increase their axial misalignment.
The most important magnetic force acting on the first coil of the anti-solenoid is an axial force F_z of $7.0{\cdot}10^6$ N, pushing it away from the interaction point and the main solenoid. Also, the structural analysis allowed to determine, under the very simple assumption of isotropy, the stresses generated inside the coil: the resulting maximum stresses are σ_{zz} = -43 MPa, $\sigma_{\theta\theta}$ = -79 MPa and σ_{rr} = -15 MPa. Figures 7a, 7b and 7c show the maps of the three principal stresses for coil number 1, while figure 7d shows the deformed shape of the whole anti-solenoid. It can be noticed that all the coils are radially compressed.
From the magnetic shielding point of view, it was evident that the most important coil of the anti-solenoid is the first one (the closest to the IP), as in the innermost part of the QD0 region the magnetic field coming from the main solenoid is stronger, and more difficult to contrast than in the other zones. In fact, it is relatively easy to obtain low values of the remaining magnetic field in the center of the QD0 region.

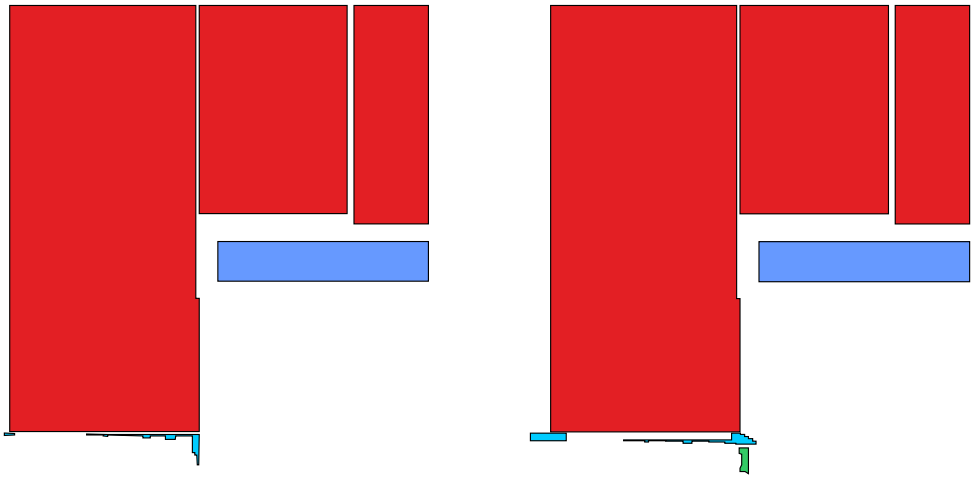

(a) Opera2D™ first version. (b) Opera2D™ second version.

Figure 8: The first Opera2D™ models.

Finally the option of having a supporting tube made of a ferromagnetic material was discarded after running a simulation in which it was modelled. That simulation pointed out how such a solution leads to an increase of the anti-solenoid currents and a higher value of residual field in the innermost part of the QD0 region, without adding any evident advantage.

2.3. The Opera2D model

As expected, the most relevant result of the Ansys™ analysis came by the force estimation. Magnetic forces are high and capable of causing instability issues, but even if it will be challenging to design a cryostat capable to withstand such loading, for that stage this was considered *feasible*.
The most stringent requirements, still unsolved at that stage, were linked to the residual magnetic field, because even the lowest values of the remaining field obtained up to this point in the QD0 region were considered high enough to perturb the final focus correct functioning. It was then decided to focus only on the magnetic aspect while improving the anti-solenoid design and postpone all the structural analyses to a following stage. Therefore, Ansys™ and the possibility to perform a mechanical analysis of the coils were abandoned in favour of Vector field Opera2D™, a program more oriented to magnetic simulations in two dimensions.
With respect to the previous Ansys™ model, we also introduced some parameter changes occurred in the meantime in the MDI layout studies. The most relevant was the machine parameter L^* which passed from 3.8 m to 3.5 m. Consequently the flux-return yoke dimensions was reduced as the whole detector became more compact. Also, the maximum anti-solenoid current density was recommended not to exceed $4.0{\cdot}10^7$ A/m^2 by

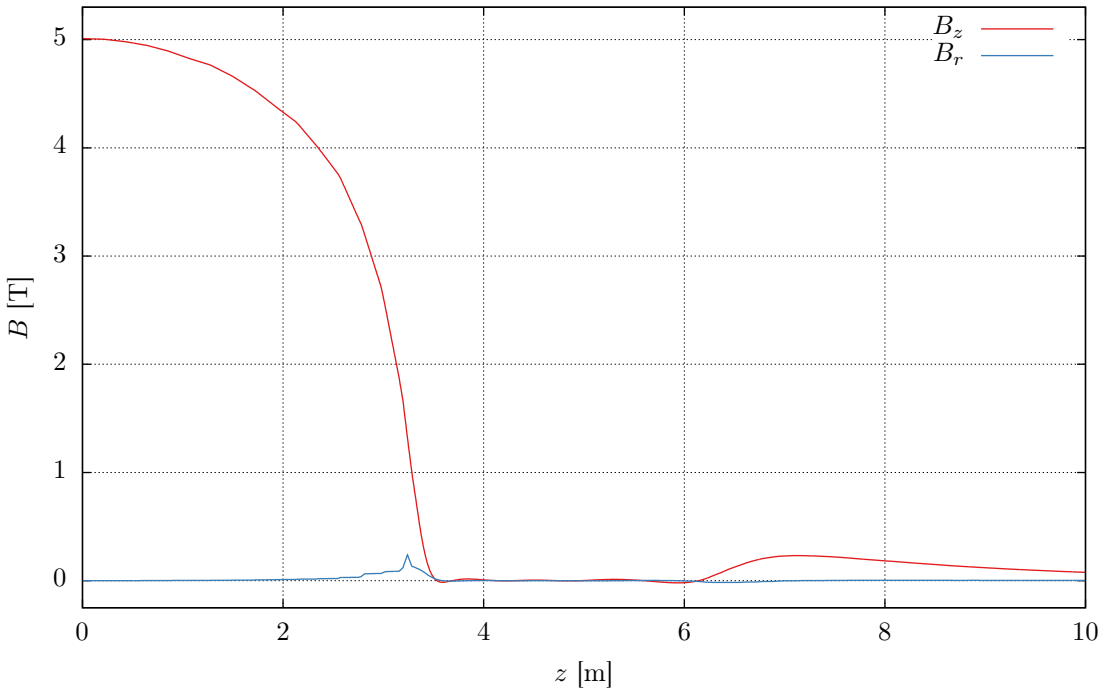

(a) Axial and radial magnetic field on the beamline.

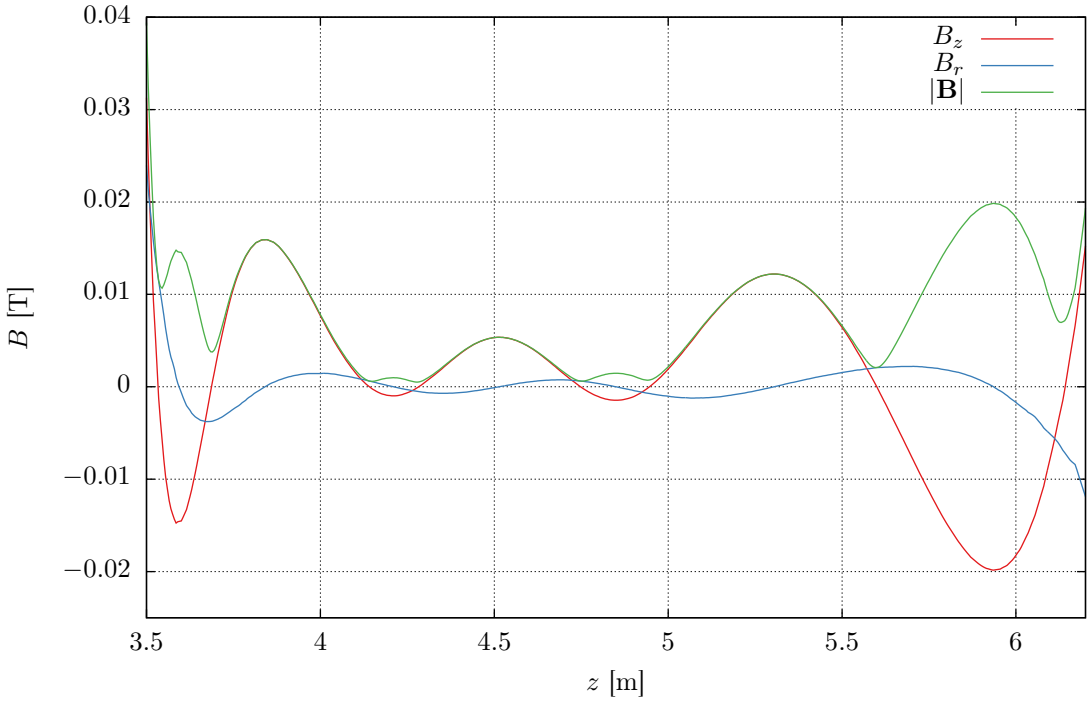

(b) A zoom in the QD0 region.

Figure 9: Field on the beamline, first Opera2D™ design.

the detector colleagues. This was considered as a safe technological limit for a solenoid of the size of the ones in the anti-solenoid.
For the very first analysis in Opera2D™, it was then decided to fix the current density value to the maximum allowed, and then modify the shape of the anti-solenoid coil section. By doing this, it was possible to literally *place* the current only where needed, so that the anti-solenoid shape visually represented where it was necessary to have more current. In addition, the overall dimensions of the anti-solenoid resulted to be smaller. In conclusion, such "free hand", trial and error approach helped to understand the magnetic behaviour of the detector, as we could literally see where it was better to have more current.
The first FEM Opera2D™ model, had a mesh made of quadratic, tetrahedral elements, with the usual option of axial-symmetry. Steel properties were the same used in the Ansys™ model, so the analyses were still non linear, and QD0 was not introduced yet.
The first evolution of the design with this new program is represented in figure 8a. In this layout the anti-solenoid section is made of just two coils with a rather complex shape and the same current density, to have the whole anti-solenoid powered by one single source. Such shapes are the result of the trial and error and manual adjustment of the section previously anticipated.
The resulting field profile on the beam-line is better than the one obtained from every previous simulation, as shown in figures 9a and 9b, even if it was present a sharp peak of B_r in the region of 3.2 m and the value of B_z outside the detector raised.

2.3.1. The ferromagnetic disc

The previous design was presented to the MDI Working Group meetings, to both have an internal review and check all the integration aspects. Some modifications were asked: it was evident that the small radius of the front part of the anti-solenoid would have interfered with the supporting tube, and it was preferred to change the anti-solenoid rather than the tube itself, because that would have led to other conflicts regarding the assembly sequence. It was then decided to remove the anti-solenoid part which was interfering with the supporting tube and replace it with a *ferromagnetic disc*, to be fixed inside the supporting tube, with the intention to create a "barrier" for the magnetic field. Such ferromagnetic disc could in fact help the field to flow in the iron end-cap before entering the QD0 area, by providing a sort of easy path, due to its low magnetic reluctance. Also, it was investigated the possibility to take some space from the adjacent Hadronic Calorimeter, by extending the anti-solenoid towards the Interaction Point, beyond the limit of the return yoke. Such study was performed because the previous analyses pointed out how important is the first coil from the magnetic shielding point of view, so it was considered interesting to take some space from the less exposed region of the calorimeter to extend the first coil of the anti-solenoid. Figure 8b shows the schematics of this new layout.
In this layout it can be seen a second, big anti-solenoid coil at the end of the QD0 area, protruding outside the end-cap. Such coil had a current density of $3.0 \cdot 10^6$ A/m^2, which is compatible with a normal conducting option. More precisely, it was chosen such a low

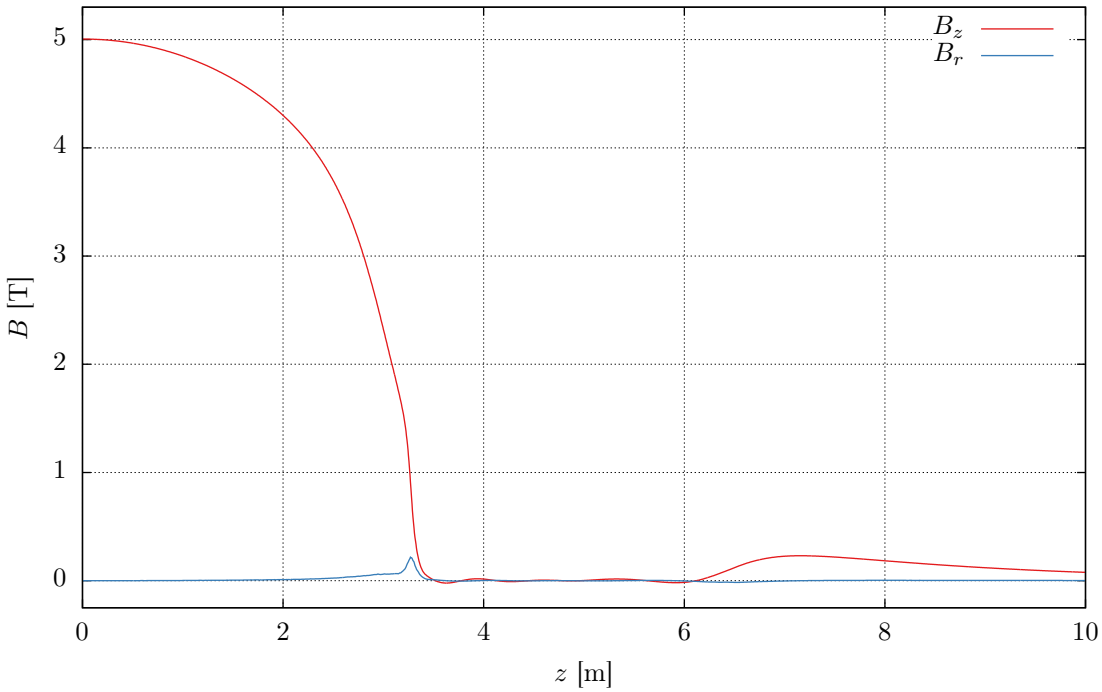

(a) Axial and radial magnetic field on the beamline.

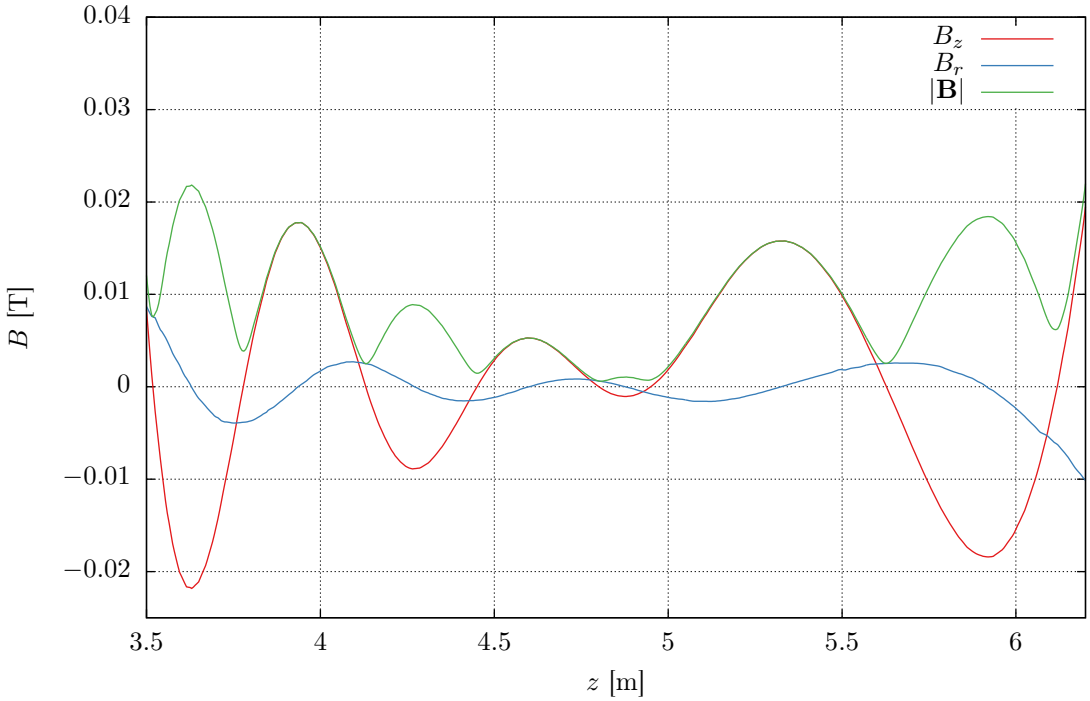

(b) A zoom in the QD0 region.

Figure 10: Field on the beamline, second Opera2D™ design.

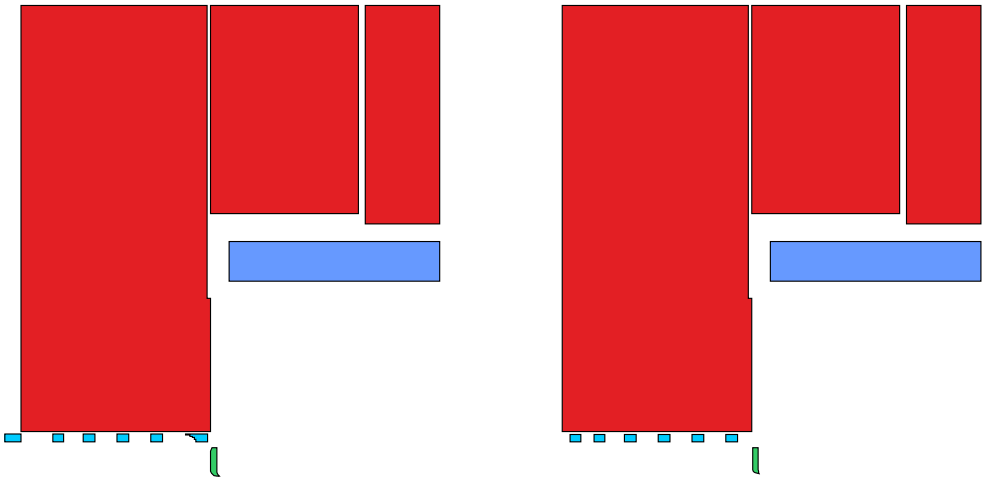

(a) Opera2D™ third version. (b) Opera2D™ fourth version.

Figure 11: The latest Opera2D™ models.

value of current density to demonstrate that a normal conducting coil could be sufficient to expel the magnetic field from the end of the QD0 area, given the possibility to have bigger coil dimensions.
In conclusion, the impact of such modifications on the field profile along the beam line can be seen in figure 10a and 10b. With respect to the previous ones, it was possible to maintain almost the same low values of the residual field, with a design compatible with the supporting tube.

2.3.2. The automated field minimization

This second Opera2D™ version was presented to the MDI Working Group meetings, to check the integration of the new design. The Detector Physics colleagues realized that an anti-solenoid which extends into the calorimeter region is not acceptable, even if the space affected is relatively small and peripheral. The ferromagnetic disc was accepted, but its dimensions needed to be revised to not interfere with the neighbouring components, mainly with the vacuum pipes. Finally it was agreed to leave 40 mm of space between the anti-solenoid superconducting coils and the surrounding systems, and reserve this space to the cryostat. Finally, it was considered safe to increase the current density in the anti-solenoid up to $8.0 \cdot 10^7$ A/m^2.
Consequently to those inputs, the space allocated to the anti-solenoid was basically imposed by the other systems, so it was not possible any more to improve its performance by finding the best shape of the coils section. It was then decided to go back to a simple design made by a sequence of coils, as shown in figure 11a, and then put an additional effort to find the best current densities to operate each single coil. It was in fact defined a numeric routine to implement an iterative process to find the currents which minimize

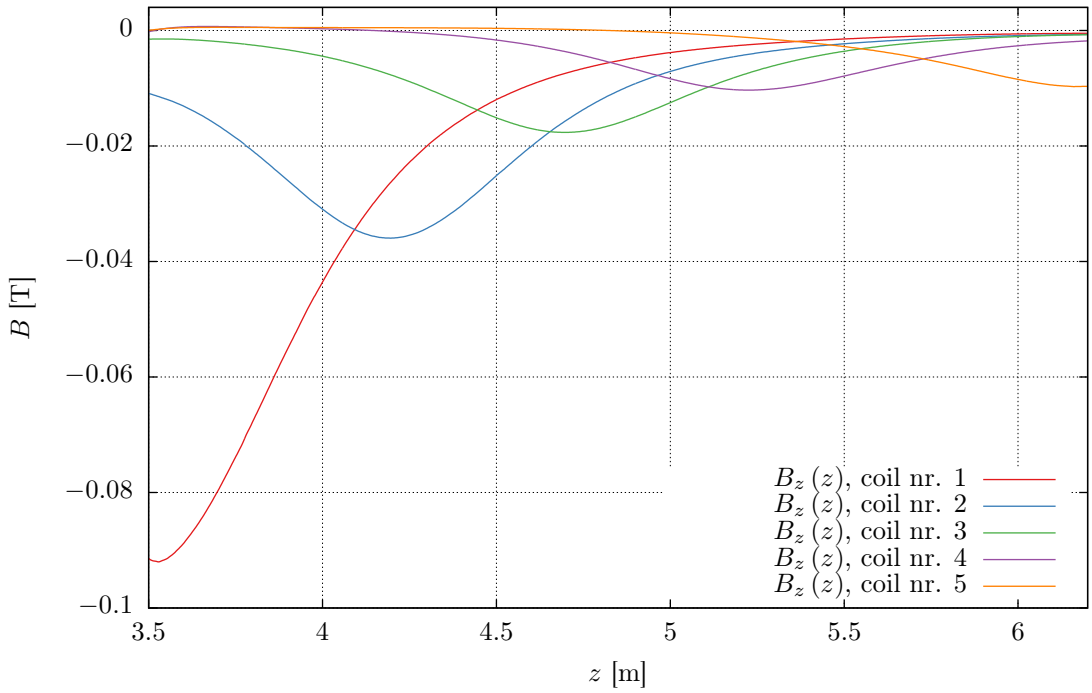

Figure 12: The coils relative contribution to the field along the beam line.

the remaining magnetic field along the beam axis in the QD0 region.
Even if the presence of the iron end-cap around the anti-solenoid makes this problem slightly non linear, a technique based on the superposition of effects was proposed and applied to the anti-solenoid in the case of nominal operating currents, assuming that in such condition, a small variation of the currents leads to a change in the magnetic field profile that can be considered linear.
Such approach is relatively easy to implement in a numeric routine: firstly the anti-solenoid is defined in the FEM software environment. The current densities and the coils number and positioning are chosen by a trial and error process, which consist in a series of simulations with a progressive adjustment of the design parameters. As soon as this method stops giving improvements in terms of remaining magnetic field in the QD0 region, the design obtained is saved and the field profile along the beam axis is stored. This field profile is saved as a discrete function $B_z(z)$. Then, for each coil is run a different, dedicated simulation, in which the coil investigated is operated at 101% of its nominal operating current, while every other coil current is set to its nominal value. The resulting field along the beam axis obtained for each coil is then saved as ${B_z}^i(z)$ where i is an index which represent the number of the coil that was perturbed. Finally, an equation in i variables (a_i) is defined as:

$$B_{int} = \int_{z_1}^{z_2} \left| B_z(z) - \sum_i \left(a_i \left({B_z}^i(z) - B_z(z) \right) \right) \right| \mathrm{d}z \tag{1}$$

where z_1 and z_2 are the boundaries of the region in which the field will be minimized (this region is slightly bigger than the QD0 region itself).
The terms ${B_z}^i(z) - B_z(z)$ are the contributions of the i-th coil to the field along the beam axis, relative to an 1% increase of the current. To have a graphical representation these terms have been plotted in figure 12 for an anti-solenoid design made of 5 coils.
This value B_{int} was then minimized in a_i using a routine for multi-dimensional minimization provided by the GNU scientific libraries [5], and the obtained values of a_i corresponding to the minimum remaining field on the beam axis were used to correct the operating currents. Just to give an example, a value $a_2 = -3.5$ meant that for the coil number 2, current has to be reduced by 3.5%.
Applying this technique, *always* produced an improvement of the anti-solenoid performance, as the remaining field in the QD0 region always decreased after adjusting the coil currents with this technique. Another important improvement came from the higher current density allowed in the first coil, and this tendency was confirmed by the numeric routine, which always suggested to increase the current on the first coil of the anti-solenoid, even beyond the maximum allowed, so that the first coil current was always set to maximum and it was no more included in the numeric routine.
However, the results obtained in this stage depended highly on the limitation that were imposed by the surrounding systems of the MDI area, up to the point that the new limitation surpassed the improvements in term of overall impact on the performance. Therefore, the remaining field on the beam axis increased with respect to the previous case, as represented in figure 13a and 13b.
In the MDI meeting that followed, those results were accepted as a consequence of the MDI evolution itself, as from this point on the status of the design was considered to be close to the final one. In particular, the design was considered mature enough to proceed with a simulation in three dimension, however a last integration step was performed before moving to the 3D.

2.3.3. The final overall integration

The results from the previous stage were presented at the recurring MDI Working Group meetings, and there some observation were raised: it was noticed that the anti solenoid could not protrude from the detector into the BDS tunnel, as this configuration is not compatible with the detector "roll-in", which is tangential to the tunnel and therefore the anti-solenoid had to be be contained inside the iron end-cap limits. Also, an updated design of the QD0 alignment system foresaw to utilize some of the space reserved to the anti-solenoid first coil (the closest to the IP). Consequently, it was necessary to move back the first coil and move forward the last coil, as shown in figure 11b. Finally, it was necessary to reduce furthermore the ferromagnetic disc dimensions.
The anti-solenoid and the disc were then modified to satisfy those new requirements, but even if the currents were adjusted, and the numeric minimization was run again in the new conditions, it was only possible to *limit* the negative impact caused by those additional space reductions. Figures 14a and 14b show the last results obtained, in the case of an MDI layout completely integrated, as presented in the CLIC Conceptual

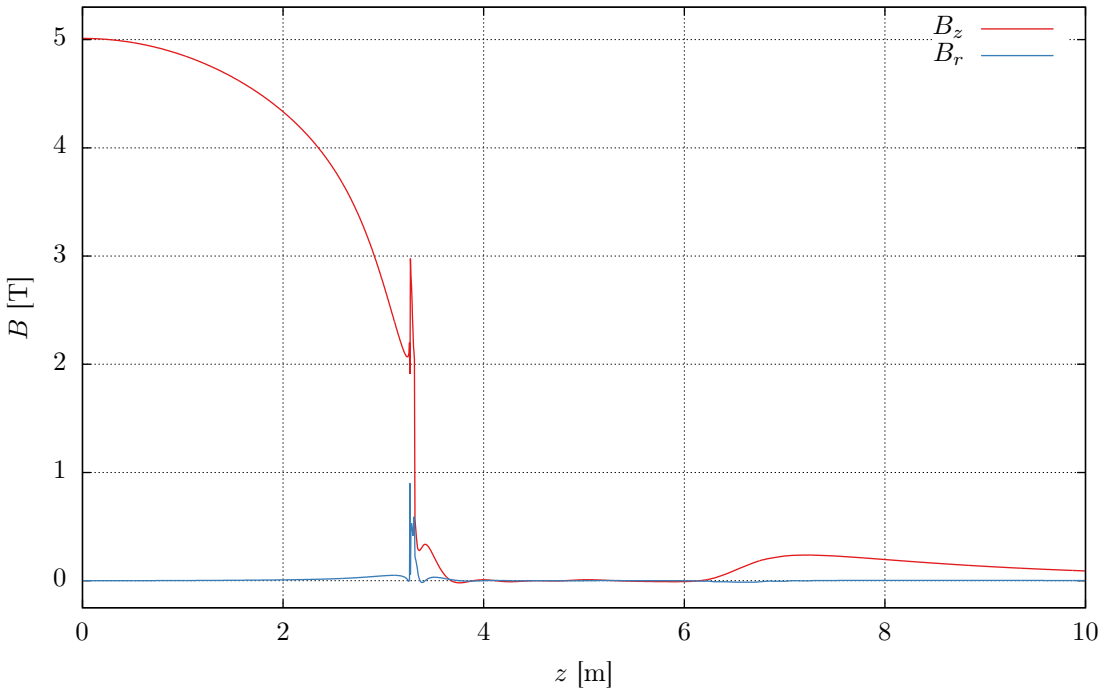

(a) Axial and radial magnetic field on the beamline.

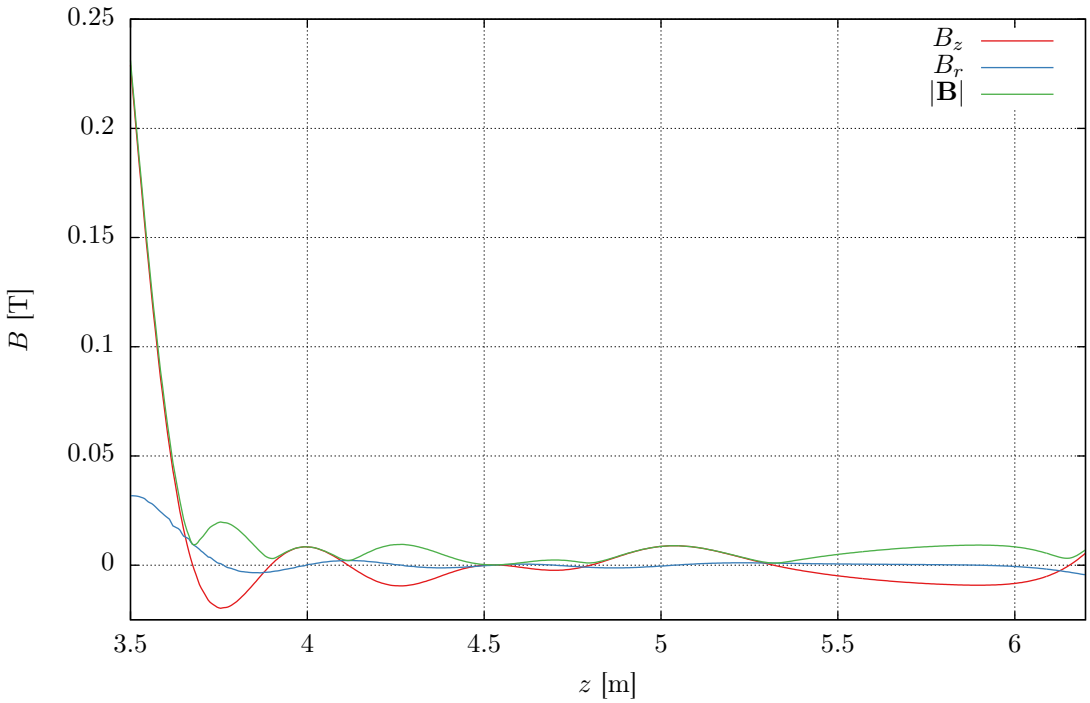

(b) A zoom in the QD0 region.

Figure 13: Field on the beamline, second Opera2D™ design.

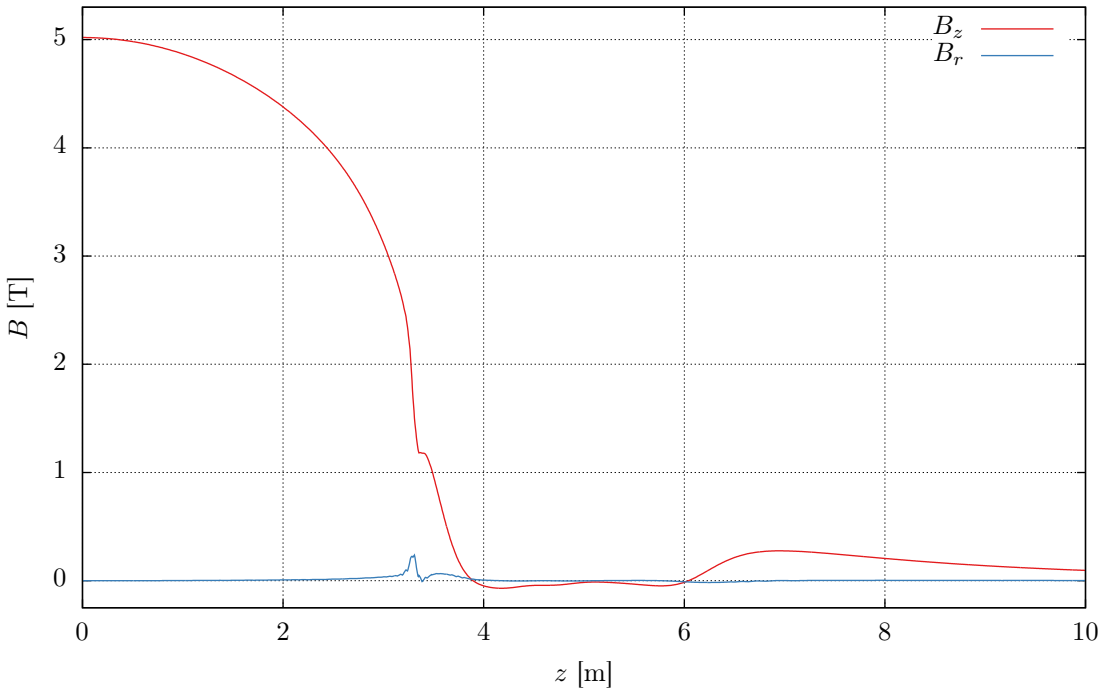

(a) Axial and radial magnetic field on the beamline.

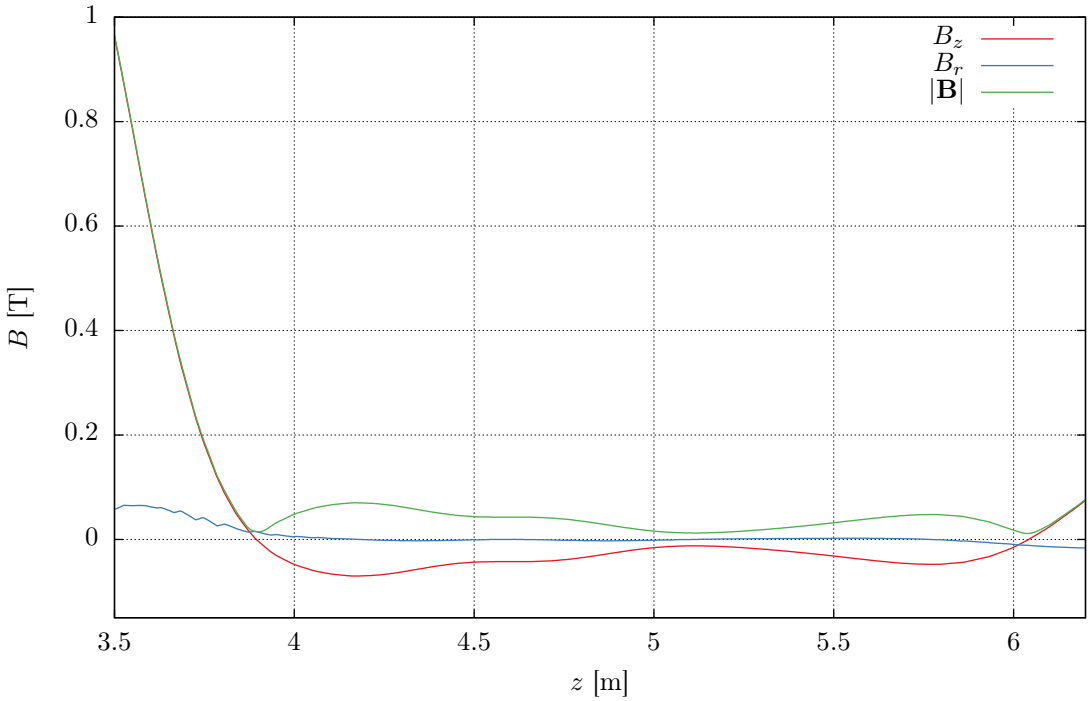

(b) A zoom in the QD0 region.

Figure 14: Field on the beamline, second Opera2D™ design.

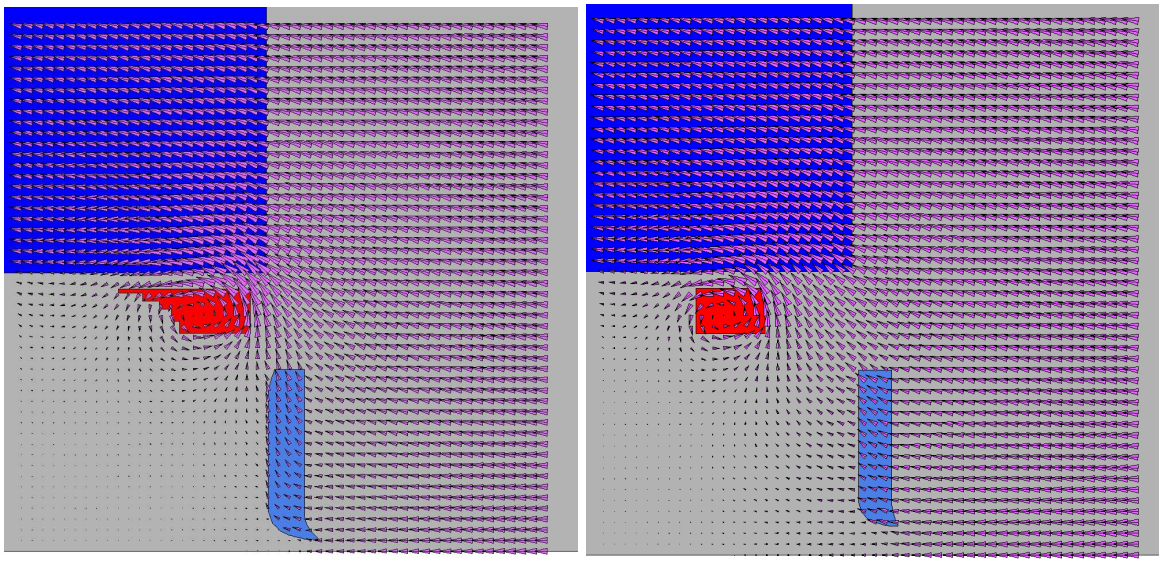

(a) Magnetic field vector map, third version. (b) Magnetic field vector map, fourth version.

Figure 15: Field maps for the last Opera2D™ models.

Design Report (CDR). Figure 15 shows a comparison between the field maps obtained by the last two Opera2D™ models, in particular Figure 15a refers to the case presented in 2.3.2, while Figure 15b refers to 2.3.3.
The latest modifications did not went in the direction of improving the anti-solenoid performances, and the values of magnetic field of this scenario were considered sufficient to influence the QD0 behaviour, but since the MDI design was *frozen* from this point on, it was perceived that the 2D model had already given everything it could in order to dimension the anti-solenoid. It was then decided to switch to three dimensional simulations, to finally include the QD0 and solve the issues still open with the appropriate model.

2.4. Conclusions on the two dimensional model

The 2D model permitted to reach numerous achievements in the dimensioning process of the anti-solenoid system. The design obtained by this model was in fact *integrated* with all the MDI system and *optimized* by a numerical minimization routine. Furthermore this model permitted to evaluate some alternative ideas such as the ferromagnetic disc and the ferromagnetic supporting tube. Such model was also used to evaluate *forces and stresses* acting on the superconducting coils, and could still be used when the transient analyses will be required to dimension the solenoids cables and their power damping system.
On the other hand, with a model as simple as this, it was not possible to determine the effective impact of the main solenoid on the final focus quadrupole QD0, and when the

MDI parameters were frozen, and the anti-solenoid performance stopped improving, it was decided to abandon the 2D model in favour of a 3D one, to finally understand if QD0 could be able to function properly in the perturbed environment of the CLIC MDI region. If not, the three-dimensional model would also be the only tool to solve such issues.
On a more conceptual basis, it confirmed that the most critical part of the anti-solenoid is the innermost (the closest to the IP), as that is the most difficult region to shield, and the one in which the highest Lorentz's forces appear. This means that the first coil is the most important of the anti-solenoid and the QD0 region could benefit remarkably of every increase of its maximum current density as well as every increase of the space reserved to it towards the IP.

3. The three-dimensional model

Considering the conclusions which followed the 2D model study, the next step naturally consisted in a three-dimensional FEM analysis, simulating the whole MDI region. In this kind of simulation in fact it can be represented not only the detector with its anti-solenoid, but QD0 as well. In addition to that, the return yoke can be modelled with its correct dodecahedral shape.
Summarizing, the main advantages presented by the 3D model were:

1. The possibility to investigate on the magnetic relation between the final focus magnet, the main solenoid of the detector and the anti-solenoid.

2. A more realistic field map along the beam line, which takes into account the presence of the iron dominated QD0.

3. The possibility to confirm the forces estimated during the 2D analyses and also evaluate the magnetic forces acting on QD0.

4. The direct computation of the gradient developed by the final focus magnet in the perturbed environment of the MDI region.

The only disadvantage comes from the increased complexity with respect to the 2D model. This mainly translates in longer set-up and computational times, but also leads to a lesser quality of the results, in numerical terms.

3.1. Description of the model

The software used to run this simulation was Vector Field Opera3D™. Considering that QD0 generates a quadrupolar field while the field in the detector is solenoidal, and that the magnet axis is tilted with respect to the detector axis by an angle of 0.01 rad; the field to simulate is completely three-dimensional, and only one plane of symmetry can be defined: the one perpendicular to the detector axis and passing by the IP. On that plane the field is parallel to the main solenoid axis.

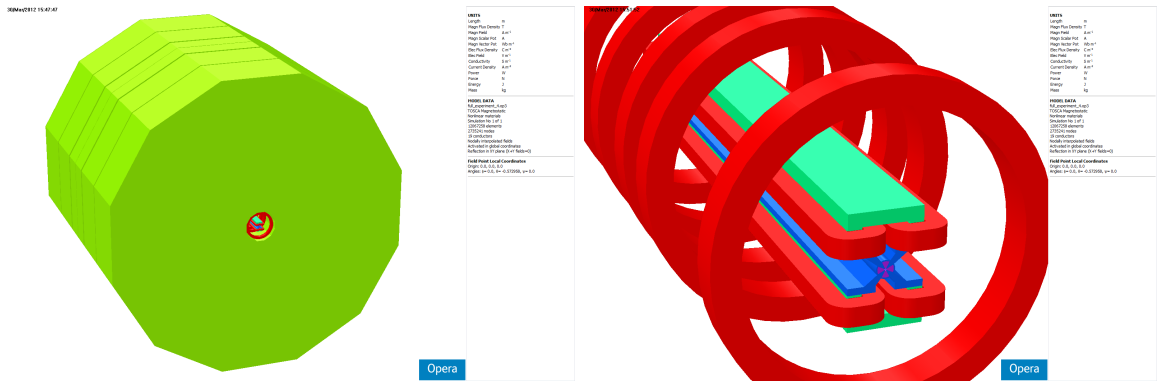

(a) Detector. (b) QD0 and anti-solenoid.

Figure 16: An overview of the Opera3D™ model.

The element type used were both linear and quadratic: linear in the detector yoke and surrounding area, to save some computational time; quadratic in the QD0 and in its region, to increase the precision of the results in the most interesting zone.
The material used for the yoke was the same as in the 2D analyses, while for QD0 three new materials were introduced: the carbon steel AISI 1010 (figure 27) used in the C-shaped return yoke, the Permendur (figure 28) constituting the pole block and finally the Vacomax-225-HR (figure 29) used in the permanent magnet blocks, as foreseen by the QD0 hybrid design [2].
The most challenging aspect of this 3D model was the scale difference between the different components of the MDI region. In the same simulation there were in fact object as big as a half of the detector iron yoke, which measures 6.2 m in length and 7 m in radius; and objects as small and detailed as the QD0 components, which has an aperture radius of just 4.125 mm. Figure 16 shows a comparison between the detector iron yoke and the QD0 surrounded by the anti-solenoid. Such difference in scale was very demanding for both the FEM software meshing routine, which was unable to create a mesh if not properly configured. In particular, to obtain a mesh which could be simulated in a few hours, it was necessary to use a relatively big element size on QD0. Such mesh permitted to obtain correctly the overall gradient achievable by the quadrupole, but because of the relatively big dimensions of the elements on the beam-line with respect to the gradient level developed in the quadrupole, the relative error on the resulting gradient was high enough to be visible: the plots show that there is always some “noise” in the fields evaluated in the QD0 region. However, despite of the bad precision of the local results, which are affected by the small number of elements in the radial direction of the quadrupole aperture; the values integrated on the magnet length are expected to be correct as they are obtained with a much larger number of elements. In conclusion, taking into account the overall level of this study as well as the level of the whole MDI region, the precision reached at this stage was considered acceptable.

3.2. Introducing the final focus quadrupole

The benefit of the new model were evident starting from the very first 3D simulation, as it clearly showed some interesting results. In particular it was evident that using the anti-solenoid design defined in the 2D simulations, QD0 was still able to attract the surrounding magnetic fields up to the point that the poles were saturated, causing a partial degradation of the magnet performances. A further adjustment of the anti-solenoid was then necessary, to prevent field from being attracted by the recently introduced magnet.
It was also evident that QD0 *shields* the beam axis: thanks to the magnet ferromagnetic body, values of B_z and B_r along the beam-line are now equal to 0 for the entire length of the QD0 region, except in the zones of severe saturation of the quadrupole itself (i.e. the innermost region, towards the IP).
Finally, it was clear that forces on QD0 can be high, if the magnet is not properly shielded. Considering the importance of such forces for the stabilization system, it was decided to follow them closely during the evolution of the 3D model.
As a last observation, the ferromagnetic disc saturated quickly, due to the higher amount of field attracted by QD0, and therefore is not advantageous any more to have it, according to the first 3D simulation. However, instead of removing it immediately, it was decided to evaluate again its performance after re-adjusting the anti-solenoid with the new 3D FEM environment.

3.3. A first adjustment

It was then necessary a stronger anti-solenoid, to compensate the effect of the introduction of QD0. Consequently, the dimensions of the coils and their operating current where increased, still maintaining all the boundaries imposed either by technical limitations or integration with the adjacent systems. This adjustment had to be done with a trial and error procedure, as the presence of QD0 made this optimization problem strongly non-linear, so the numeric routine based on the superposition of effects could not be used any more. It was also true that the presence of QD0 "distributed" the field generated by the anti-solenoid, making it less sensitive especially to coils position adjustments, and therefore easier to dimension.
Figure 17 shows the magnetic flux attracted by QD0 ferromagnetic structure, after the first anti-solenoid refinement based on the 3D model. In this simulation, the quadrupole coils were turned on, to simulate properly the usual working conditions, but in the picture is only represented B_z, which is the solenoidal component of the field and is not generated by the magnet.
In a second results post-processing the field along the beam-line was evaluated and the output is plotted in figures 18a and 18b.
Compared to the 2D case, the numeric errors (in terms of noise on the results) are much more evident. Unfortunately, such uncertain level was not possible to reduce due to convergence errors in either the numeric solver or the mesh generator, and this error was high enough to visibly affect the result of the remaining field along the beam-line. However, the tendency of the plots and the integrated values of the field confirmed the

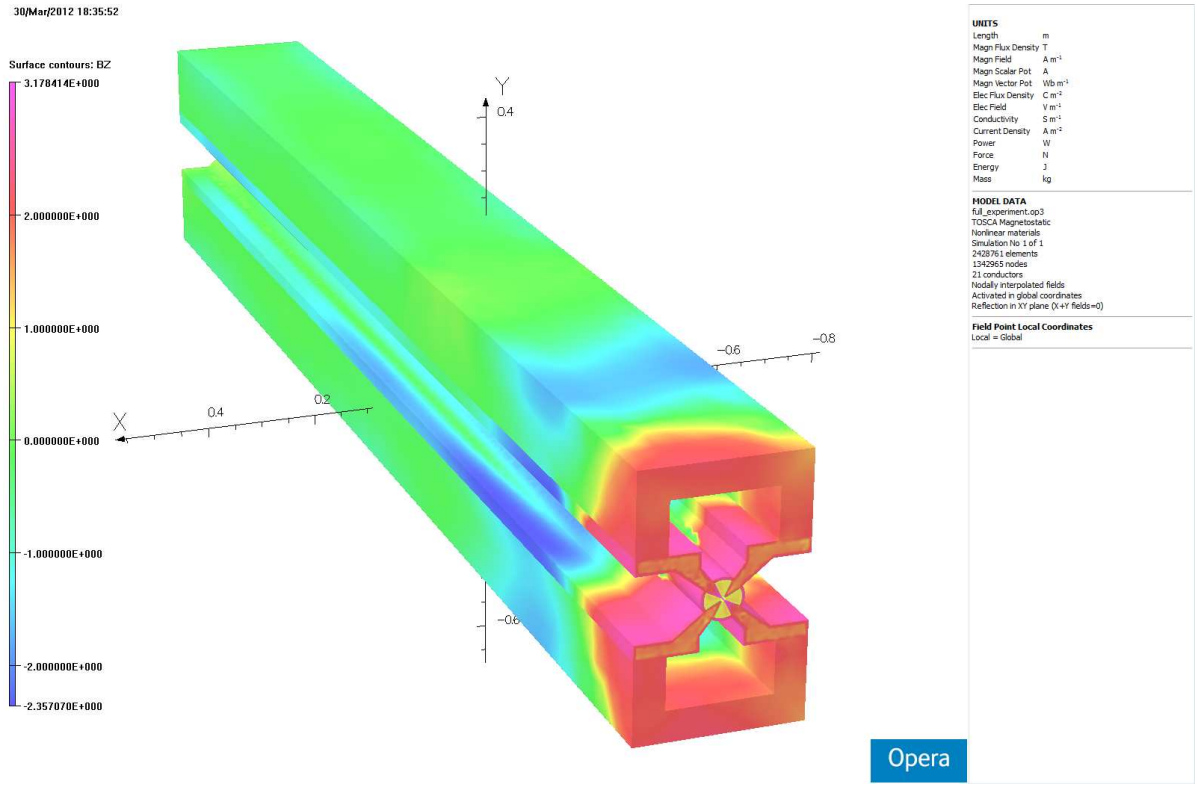

Figure 17: Axial field attracted by QD0, first Opera3D™ design.

fact that the ferromagnetic pole block tends to shield the beam-line from any external magnetic fields.

In an additional results post-processing the gradient developed by QD0 in such perturbed environment was evaluated, and the results are represented in figure 19. The gradient values were calculated along four lines parallel to the beam axis, and distant $\pm$ 1 mm from it, either in the x or y direction (in the QD0 coordinate system, in which the beam-line is directed as z, and y is directed as gravity). It can be noticed a decrease of the gradient in the innermost part of the magnet: that is to attribute to an inadequate shielding provided by the anti-solenoid, which allows too much magnetic field entering the first part of the QD0 poles, leading to their saturation and to the consequent gradient reduction.

The ferromagnetic disc was abandoned, after comparing different simulation in which it was present or not. QD0 in fact is much more influential on the field than the disc itself, and even with an anti-solenoid dimensioned using the 3D model, a ferromagnetic disc could not show any evident benefit in redirecting efficiently the undesired fields.

The magnetic forces and torques acting on QD0 were also evaluated. The most relevant were found to be $F_z \simeq 5.1 \cdot 10^4$ N and $T_y \simeq 8.4 \cdot 10^3$ Nm (evaluated in the center of the quadrupole). Such values were considered potentially problematic for the active stabilization systems required by the magnet, so it was decided to put additional efforts to improve the shielding. Not having any other real option, it was decided to investigate if

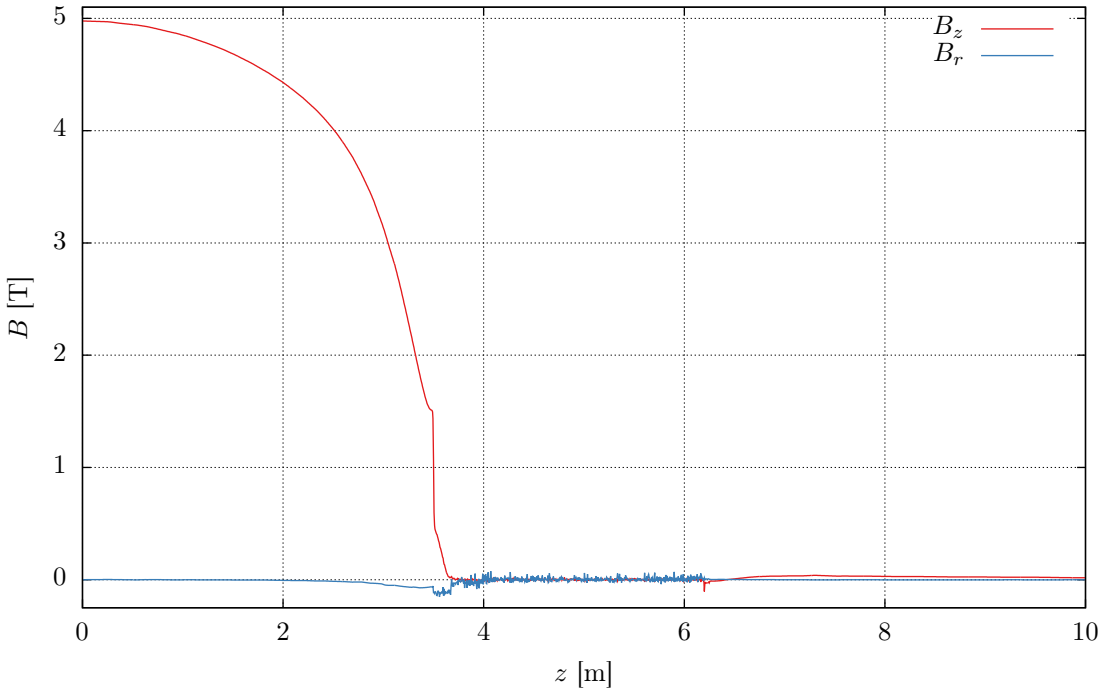

(a) Axial and radial magnetic from the IP to 10 m away.

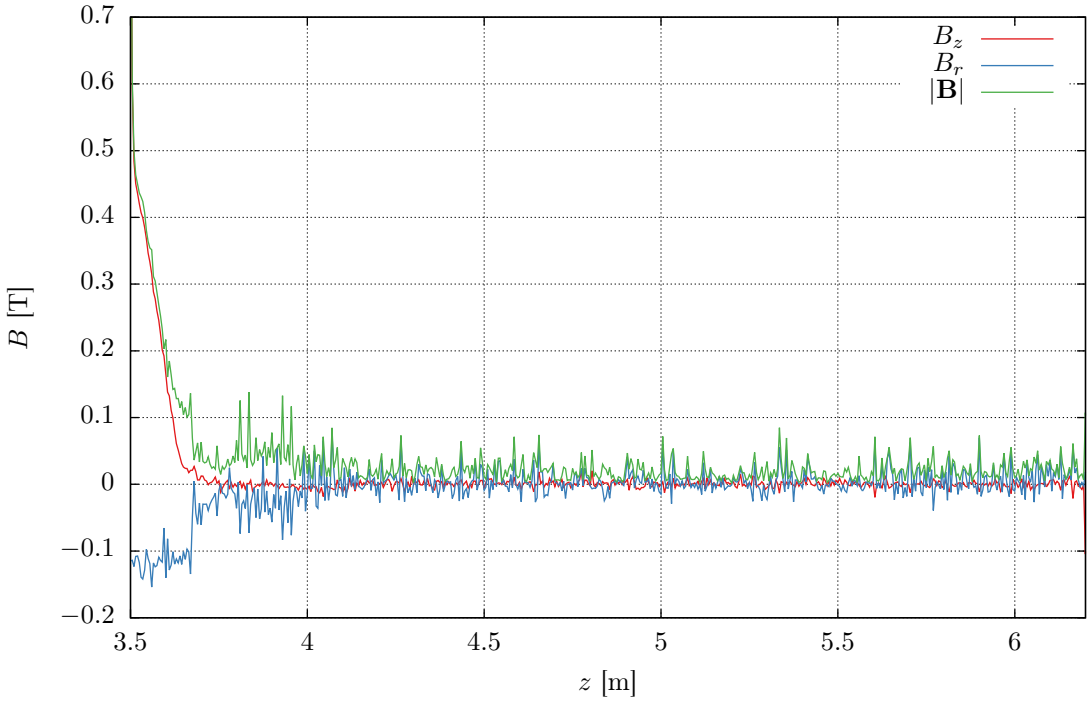

(b) A zoom of $|\mathbf{B}|$, B_z and B_r in the QD0 region.

Figure 18: Resulting magnetic field on the beam line, first Opera3D™ design.

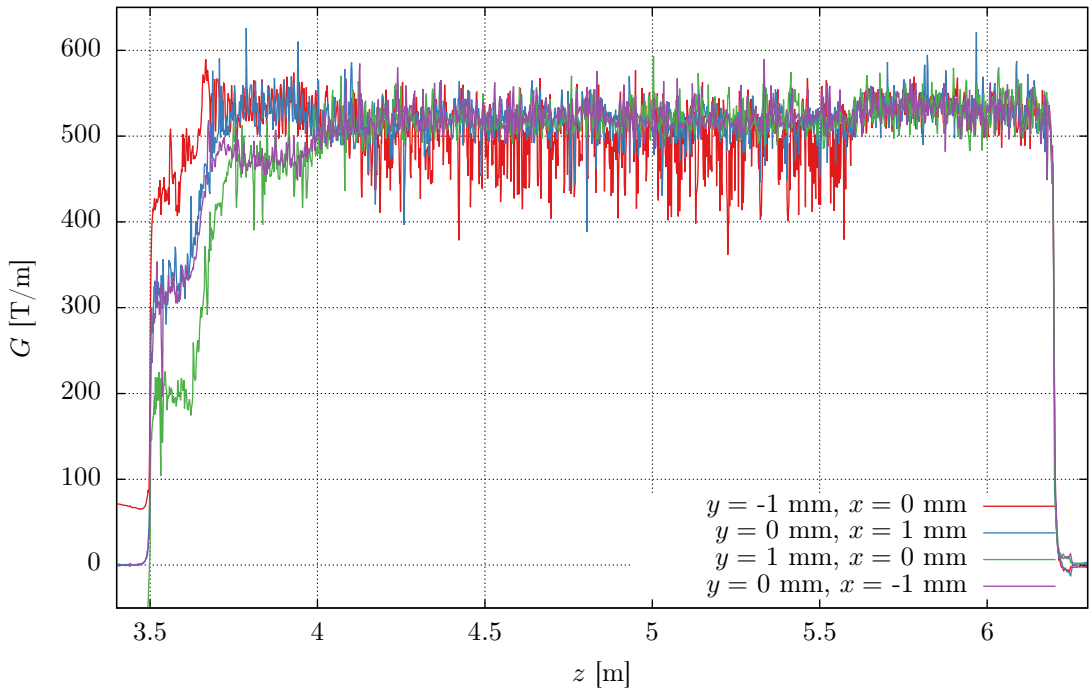

Figure 19: QD0 gradient, first Opera3D™ design.

a more efficient shielding could be obtained, at the cost of loosing a complete integration with all the surrounding system of the MDI region.

3.4. A further refinement

The results obtained by adjusting the anti-solenoid were not completely satisfactory yet, especially because it was not demonstrated so far that such shielding could protect completely the QD0 and therefore make it work as specifications. It was then decided to investigate the option of abandoning some of the integration boundary conditions, to have more space for the anti-solenoid and have the possibility to move its coils closer to the IP. In particular, to obtain the following results, some space was taken back from the pre-alignment system [6] whose schematics are shown in figure 20.
The first coil was moved towards the IP until its cryostat reached the limit of the Hadronic Calorimeter, and all the currents and positions of the coils were revised. The results in term of saturation of QD0 are shown in figure 21, while its gradient, evaluated as in the previous case, is plotted in figure 22.
An improvement from the previous case was evident, as the value of B_z decreased and the gradient increased consequently. The difference in integrated gradient obtained between this case and the reference one, defined by simulating the QD0 alone, is less than 5%. This result is acceptable by a magnet point of view, especially when considering the overall status of the MDI region design.

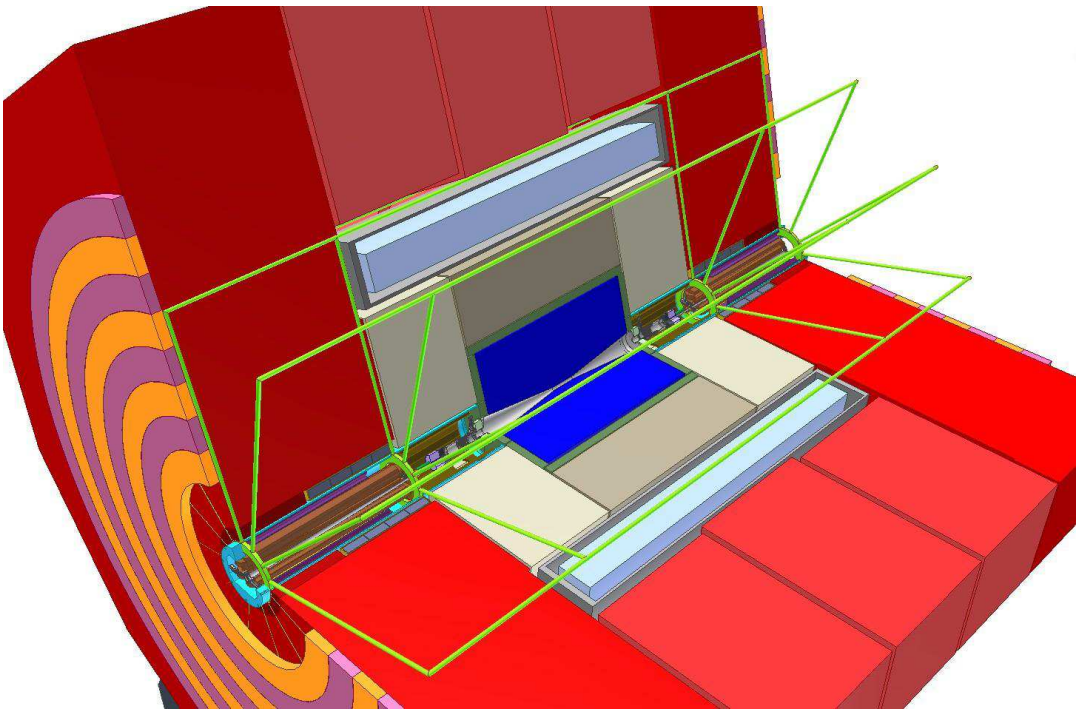

Figure 20: The pre-alignment conceptual scheme (in green).

The forces on QD0 were also reduced to a value of $F_z \simeq -5.7$ kN, $F_x \simeq 8.3$ kN and $T_y \simeq 5.6 \cdot 10^3$ Nm. A sign change can be noticed in the force in the z direction, meaning that by modifying the anti-solenoid it is possible to cancel the axial force acting on the magnet. This is not evident in the case of F_x and T_y, which are forces generated by the fact that QD0 axis is not the same as the anti-solenoid (because of the crossing angle of the beam lines). For such force and torque is more difficult to obtain a reduction, but in principle if the QD0 was completely shielded there would not be any magnetic force between it and the detector, so every improvement of the shielding leads to a reduction of the forces.
This anti-solenoid design, which dimensions and currents are reported in appendix B, was considered as the most realistic among all the designs investigated during this whole R&D study. In fact the integration incongruity was not considered overwhelming, the forces were under control, and the operating conditions of QD0 preserved. For this reason, it was decided to run some beam dynamic simulations taking into account the field profile on the beam axis obtained with this design.
Figures 23a and 23b show the field output of the 3D model, together with the interpolated values which were used in the beam dynamic simulations. In fact, considering the uncertain on this kind of results, the field maps were "smoothed", mainly to not simulate what we were sure to be numeric noise introduced by the not ideal element dimensions due to the scale issues of the FE 3D model. The smoothing was quite aggressive, but this was intentional, as we wanted to simulate the best scenario we could imagine to be able to provide with this kind of configuration, and finally understand if the solution

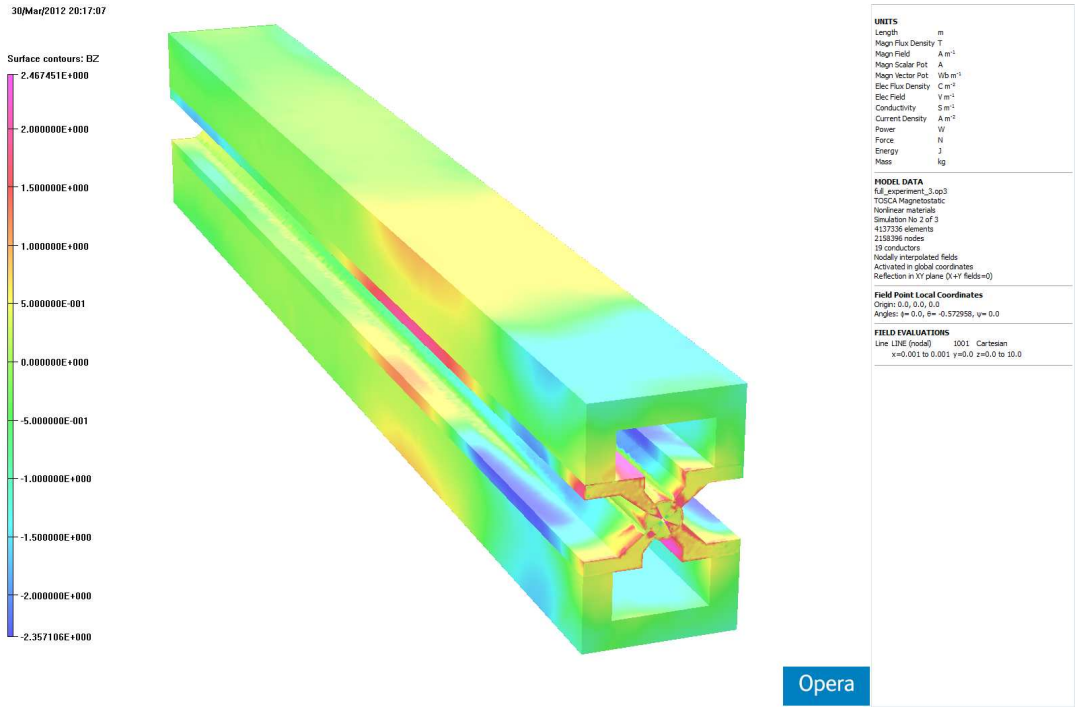

Figure 21: The axial field attracted by QD0, second Opera3D™ anti-solenoid design.

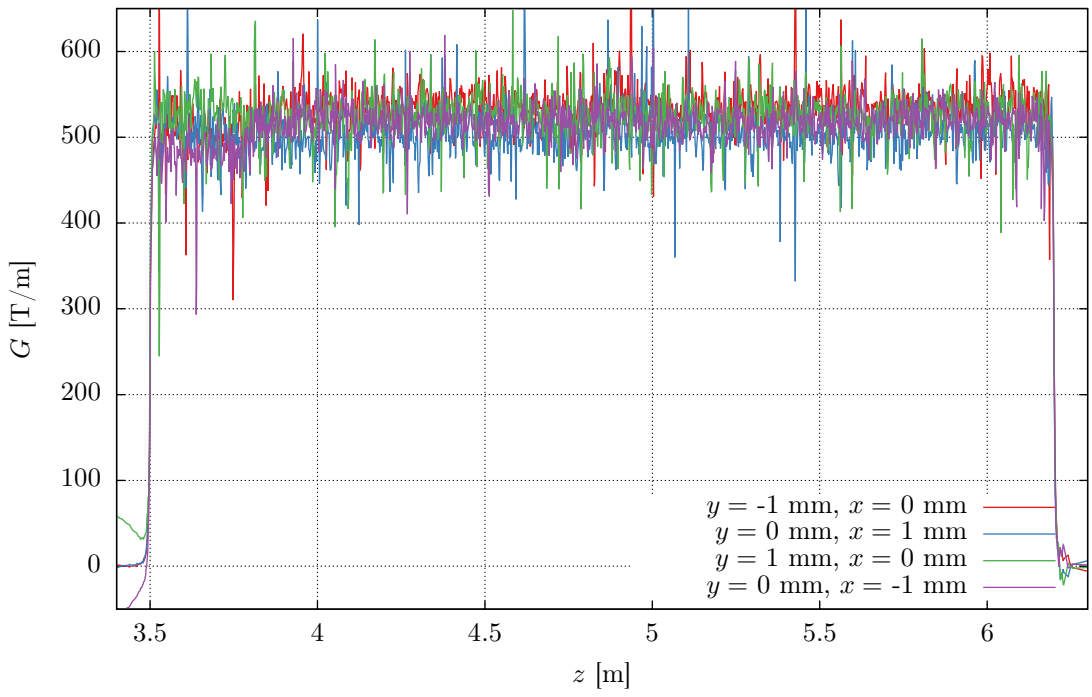

Figure 22: QD0 gradient, second Opera3D™ design.

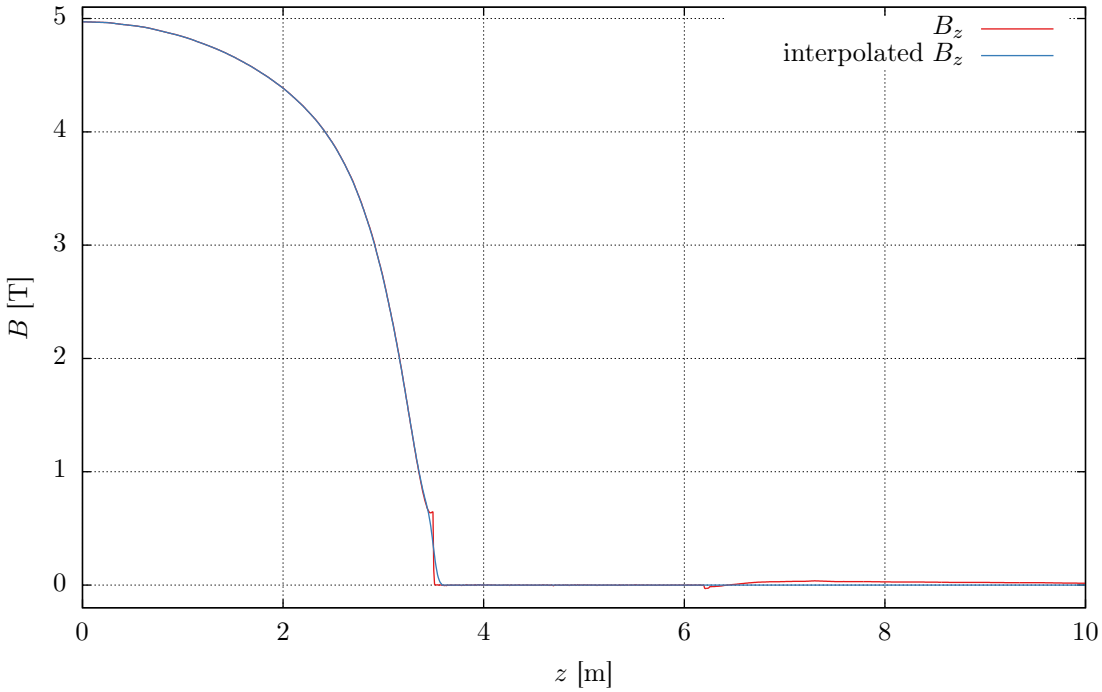

(a) Axial magnetic field from the IP to 10 m away.

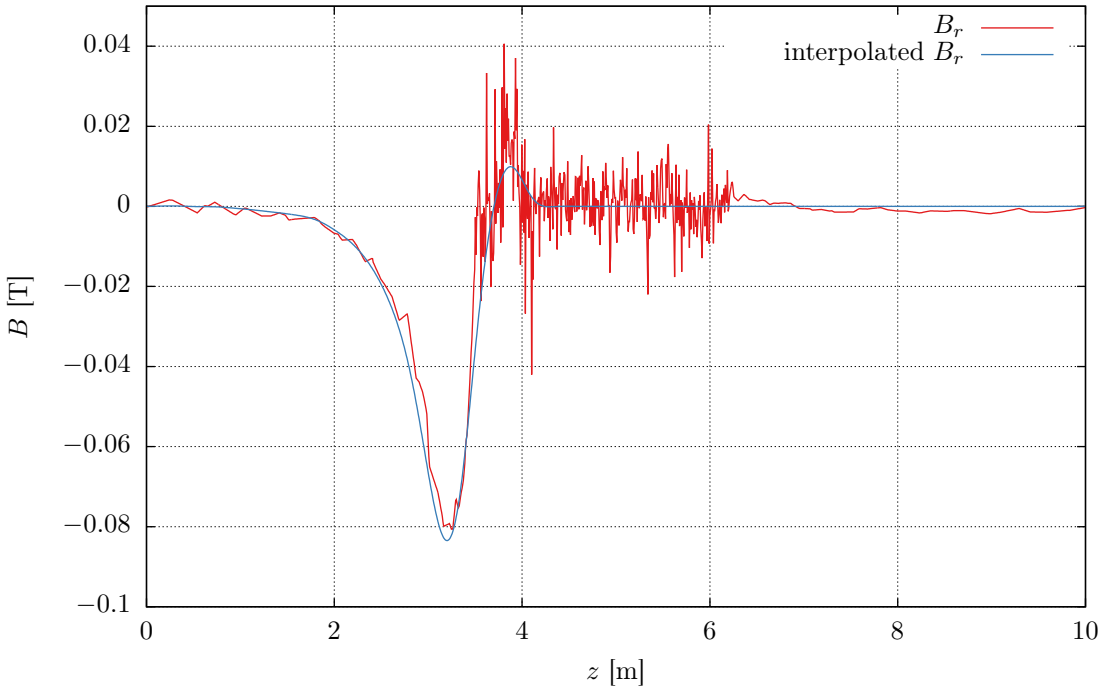

(b) Radial magnetic field from the IP to 10 m away.

Figure 23: Computed and interpolated field on the beam line, second Opera3D™ design.

based on the anti-solenoid could be validated.
The results of those simulations showed a luminosity decrease of about 14%, which is completely compatible with any other previous detector design [7]. From the beam dynamic point of view it is safe to say that the anti-solenoid solution doesn't bring any worsening with respect to the ideal case of the detector alone (i.e. no antisolenoid, and no final focus).

3.5. A last conceptual investigation

The results obtained up to this point were considered satisfactory, but it was evident that there could be an even better solution. Therefore, a last, heavier modification was introduced to show that the final focus quadrupole could achieve its nominal gradient in its whole length: QD0 was moved away from the IP by 0.3 m. In other words L^* was increased from 3.5 m to 3.8 m. It was clear that such modification would completely revolutionise the BDS design, but from the point of view of this study, the aim was to demonstrate that the anti-solenoid could completely shield the QD0, if enough space would be made available. Figure 24 shows the gradient developed by QD0 in case of an increased L^*. Such results were considered finally good, and to validate them the model was run again with the anti-solenoid and the main solenoid turned off. The gradients obtained in those two cases were then subtracted and their difference is plotted in figure 25. Having less than 1% of difference between the integrated gradient of the perturbed and unperturbed cases, which is less than the estimated accuracy of the FE model, demonstrates the effectiveness achievable by the anti-solenoid, at the cost of a more generous space allocation.

4. General conclusions and road-map

The present study and design of an anti-solenoid system for CLIC Final Focus was perfectly time-fitting the global R&D phase for CLIC Project (Machine and Detectors). In fact, the Conceptual Design Report for the CLIC Detectors [1] was recently released and the CDR of the Accelerator part is also very close to be released (a draft is available on the CLIC website `http://clic-study.org/`).
Even if the machine parameters and layout and the design of the experiments are of course not frozen and some different scenarios, mainly for the chose of L^* parameter, are still under study and discussion, it was important and worthwhile to study in detail the most challenging of these scenarios that is the SiD Detector layout with a L^* of 3.5 m.
The results obtained are very satisfactory and encouraging: all the system main knobs for the design and integration of the anti-solenoid were evidenced and investigated. Overall results are clear and positive in the sense that it seems feasible to realize a compact superconducting anti-solenoid system able to shield the hybrid QD0 quadrupole and the incoming beam region from the effect of the Detector solenoid magnet. We have now a clear idea of the most important aspects to control the performance of the anti-solenoid system and the main implication for its integration in the detector region.

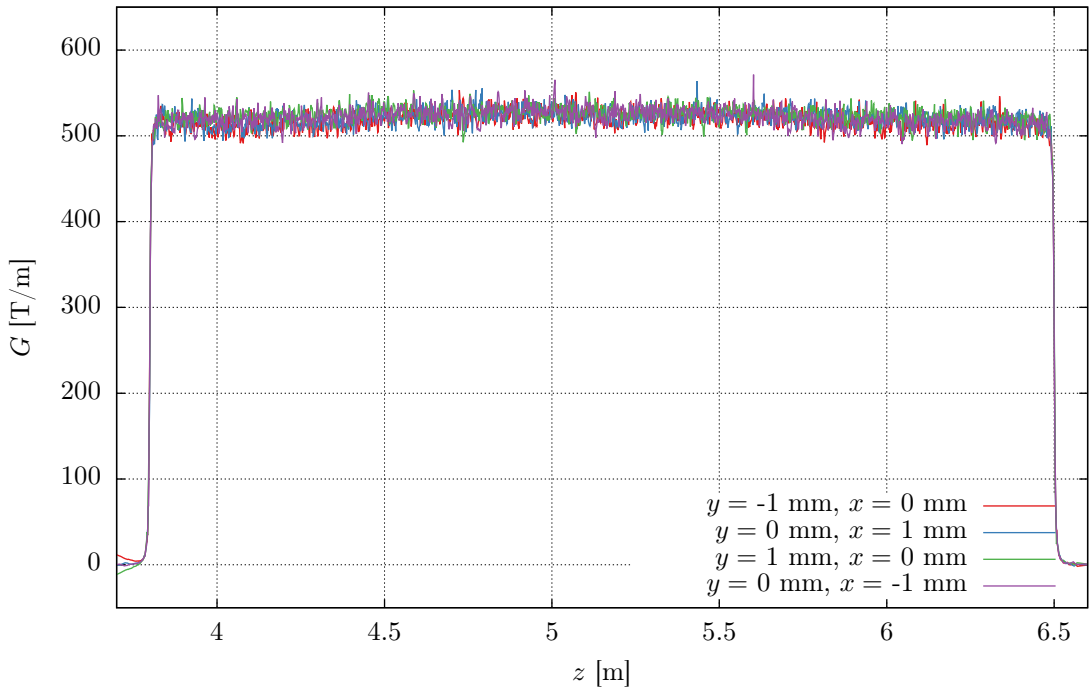

Figure 24: QD0 gradient with modified L^*.

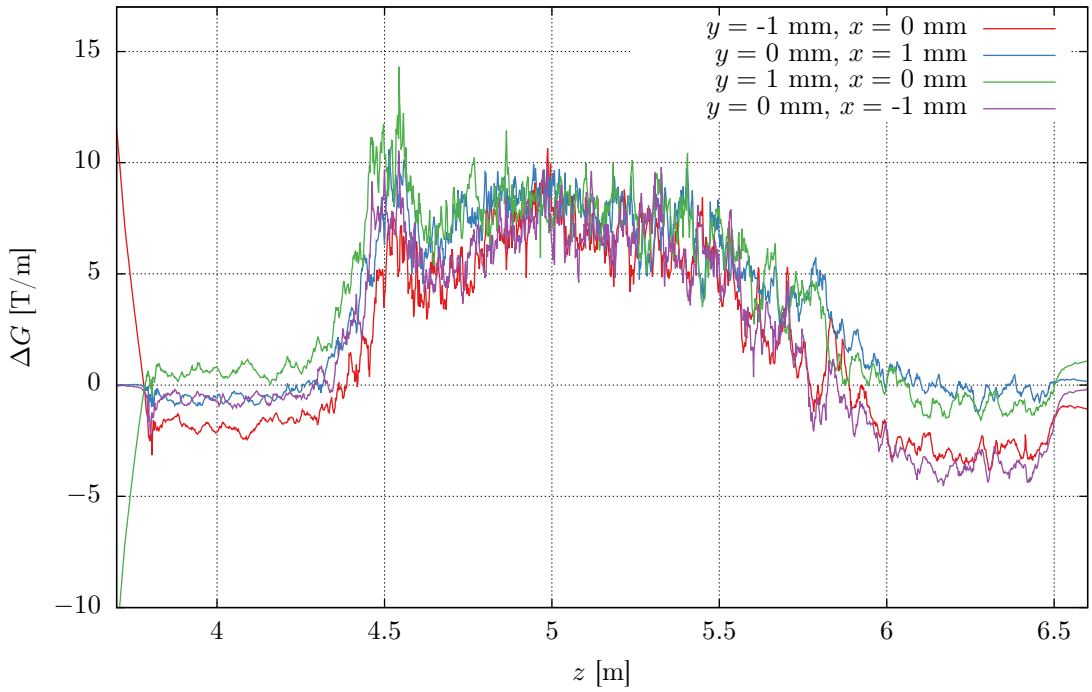

Figure 25: QD0 gradient, difference between perturbed and unperturbed case.

Starting from a 2D model, a full 3D model of the Machine Detector Interface region including all the active and passive magnetic elements was developed and is now available for further studies and checks on the most interesting layouts and configurations that will be identified by the join activities of the CLIC Machine and Experiment Collaborations.

5. Acknowledgements

This study would not have been possible without the precious contribution of all the colleagues working on the CLIC MDI team. A special thank goes to Lau Gatignon, for coordinating the MDI working group, and to the the detector team, particularly to A. Gaddi and H. Gerwig, for all the information and suggestion they gently provided about the SiD detector and the preliminary anti-solenoid designs. Not less important was the cooperation with the beam dynamics group, represented by B. Dalena, which always gave interesting feedbacks on the relationship between the beam behaviour and the remaining field.
A sincere thank goes to all of the colleagues who participated to the MDI meeting: K. Artoos, P. Burrows, H.M. Durand, K. Elsener, L. Gatignon, A. Hervé, A. Jeremie, D. Schulte, A. Vorozhtsov, and many others, who always contributed with suggestions, advices and comments on this research study, with a truly cooperative spirit.

References

[1] L. Linssen, A. Miyamoto, M. Stanitzki, and H. Weerts. Physics and Detectors at CLIC: CLIC Conceptual Design Report. 2012.

[2] M. Modena, D. Tommasini, and A. Vorozhtsov. Design and Manufacture of a Hybrid Final Focus Quadrupole Model for CLIC: presented at MT-22 Conference, 12-16 September 2011, Marseille - France. (EuCARD-PUB-2011-007).

[3] D. Swoboda. CLIC Spectrometer Magnet Interference. 6th MDI meeting, 2009.

[4] *Release 11.0 Documentation for ANSYS.*

[5] M. Galassi, et al. *Gnu Scientific Library: Reference Manual.* GNU GSL website.

[6] H. Mainaud Durand. BDS alignment progress. LCWS11, 2011.

[7] CLIC main detector solenoid and anti-solenoid impact: presented at CERN at the CLIC Collaboration Working Meeting, 10 May 2012.

Appendix A BH curves

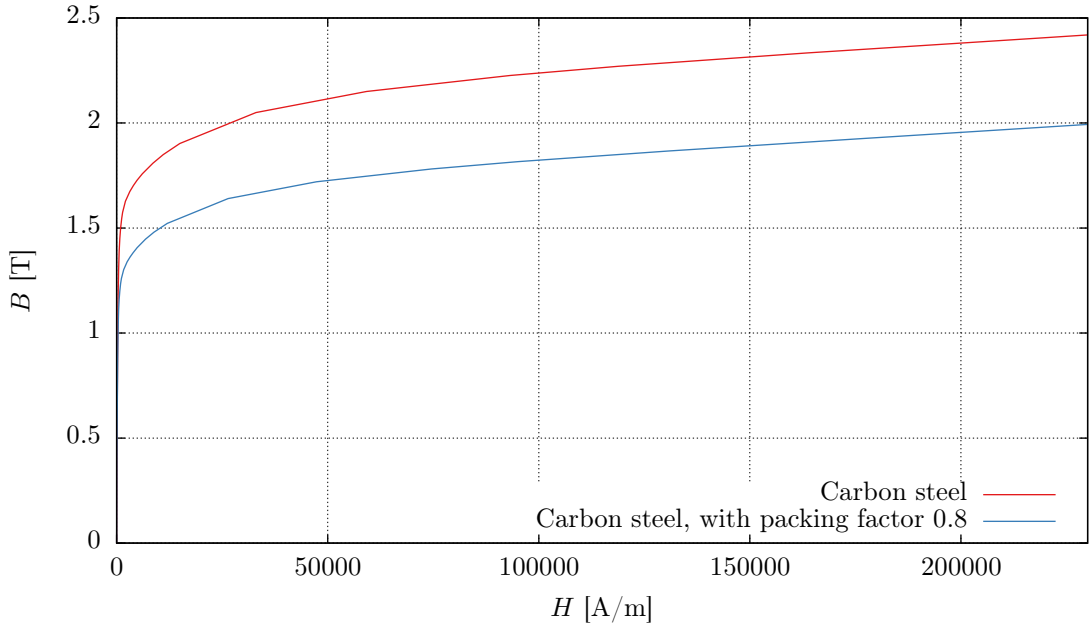

Figure 26: The BH curve used for the steel of the detector return yoke.

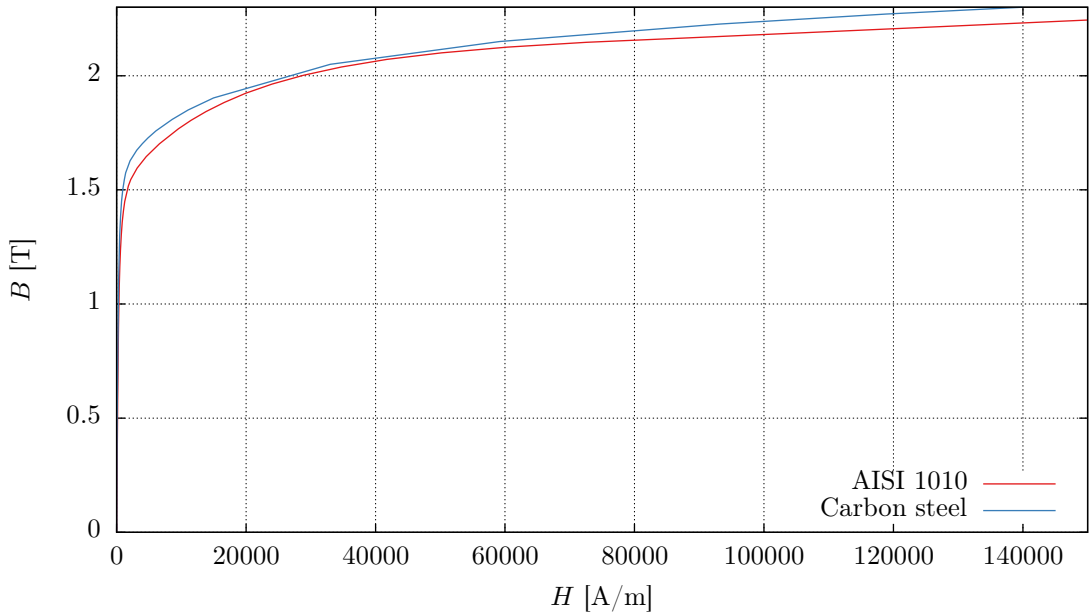

Figure 27: The BH curve of AISI 1010, used for the QD0 yoke.

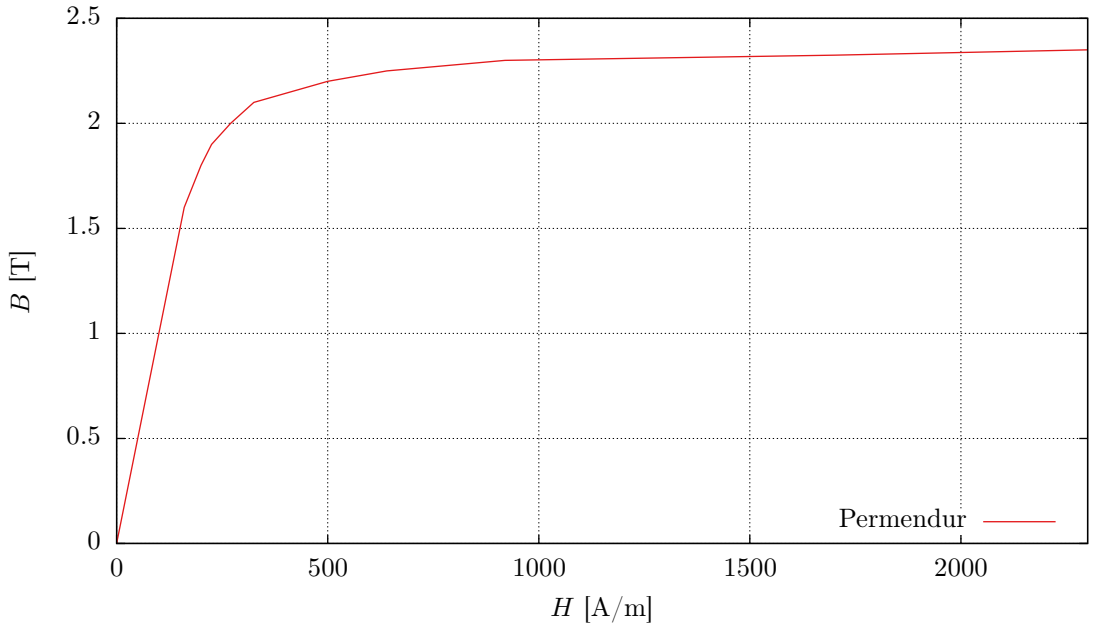

Figure 28: The BH curve of permendur, used for the QD0 poles.

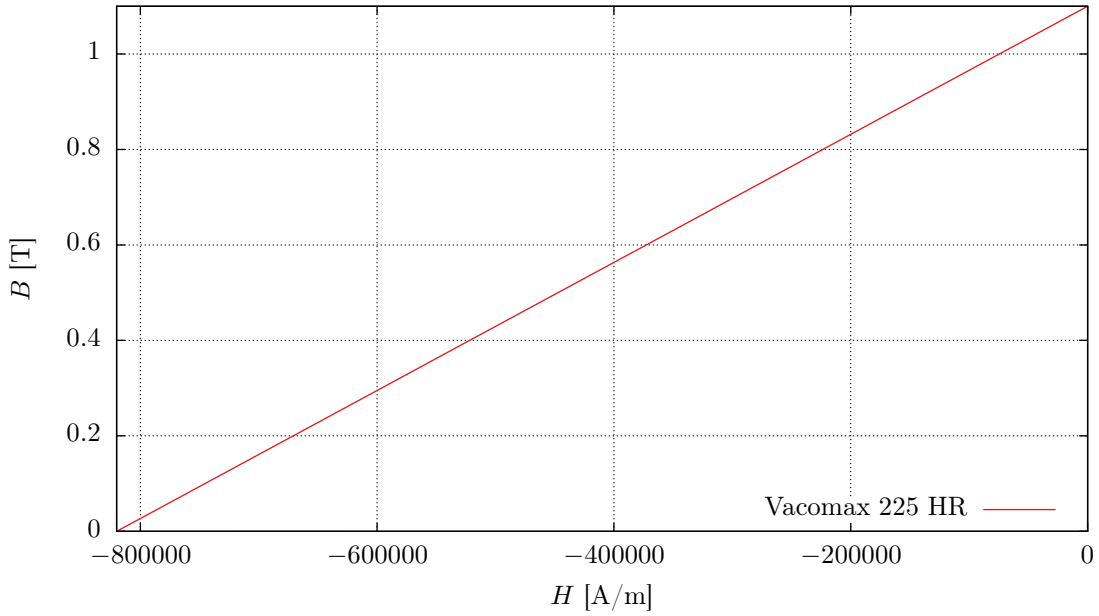

Figure 29: The BH curve for Vacomax 225 HR, used for the QD0 permanent magnet blocks.

Appendix B Final anti-solenoid dimensions

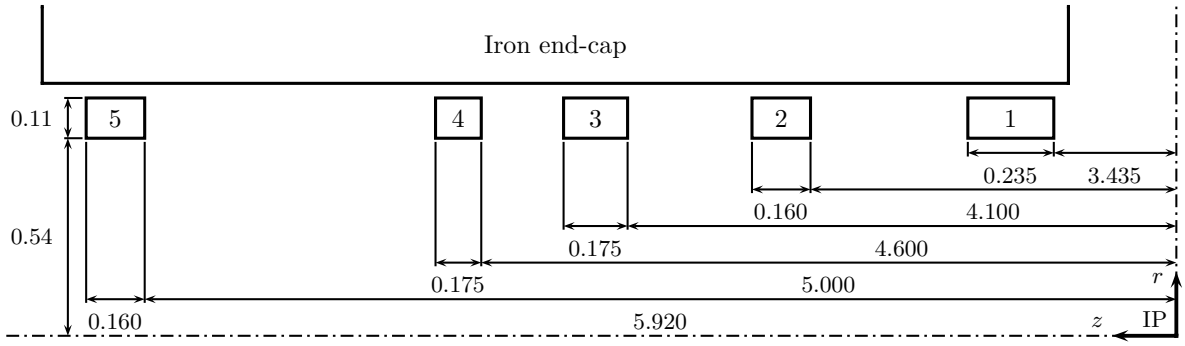

Section number	1	2	3	4	5	
Current density	80.0	23.5	15.0	3.8	2.0	$\frac{A}{mm^2}$

Figure 30: Anti-solenoid coils dimensions (in meters) and current densities.